Dynamical Climatology

The effect of a sea-surface temperature anomaly on a prediction of the onset of the south-west monsoon over India.

by

R. Kershaw

DCTN 44 **July 1986**

Meteorological Office (Met. O. 20)
London Road
Bracknell
Berkshire RG12 2SZ

DYNAMICAL CLIMATOLOGY TECHNICAL NOTE NO. 44

THE EFFECT OF A SEA-SURFACE TEMPERATURE ANOMALY ON A PREDICTION OF THE ONSET OF THE SOUTH-WEST MONSOON OVER INDIA

by

R Kershaw

Submitted for publication in Quart. J. R. Met. Soc.

Met O 20 (Dynamical
Climatology Branch)
Meteorological Office
London Road
Bracknell
Berkshire, UK RG12 2SZ

July 1986

Note: This paper has not been published. Permission to quote from it should be obtained from the Assistant Director of the above Meteorological Office branch.

THE EFFECT OF A SEA-SURFACE TEMPERATURE ANOMALY ON A PREDICTION OF THE ONSET OF THE SOUTH-WEST MONSOON OVER INDIA

by R. Kershaw

Meteorological Office, Bracknell, Berkshire

SUMMARY

At the time of the onset of the monsoon in June 1979 the sea-surface temperatures in the eastern Arabian Sea were warmer than normal. A prediction experiment designed to reveal the effects of this anomaly on the onset is described. This involves two 8-day forecasts made using the same model and the same initial conditions. They differ only in using different sea-surface temperatures in the eastern Arabian Sea. A better prediction of the onset is obtained by using the anomalously warm temperatures rather than the normal climatological values. In particular, the development of a tropical storm over the Arabian Sea, the strengthening of the Somali Jet, and the northward movement of the rainfall over India are all better predicted. The mechanism of the onset in the model is discussed and two important feedback loops are identified, one involving moisture-flux convergence and the other involving the surface fluxes of sensible and latent heat. The most important factor in both loops is the release of latent heat over the Arabian Sea. A

linear model is used to show that the onset may be thought of as a response to this heating. The roles of barotropic and baroclinic processes in the onset are also discussed.

1. INTRODUCTION

Seetaramayya and Master (1984) pointed out that the surface temperatures in the eastern Arabian Sea were warmer than normal at the time of the onset of the south-west monsoon in 1979. Their paper also contained the suggestion that the development of a tropical storm in this region was aided by the warm anomaly. Many research groups have attempted numerical predictions of the onset in 1979, the year of the Global Weather Experiment (FGGE), with varying degrees of success (Krishnamurti et al., 1983a). In particular, most attempts did not predict the formation of the tropical storm (also known as the onset vortex). Notable exceptions were the experiments by Krishnamurti et al. (1984) in which the use of an enhanced (envelope) orography led to the formation of the vortex, and the results reported by Kershaw (1985a) in which the use of modified parametrization of convection and radiation led to the formation of the vortex. However, even these relatively successful predictions failed to simulate the strength of the circulation of the vortex. As far as can be seen from published results, all of these earlier prediction experiments used climatological estimates of sea-surface

temperatures, rather than observed values. If the sea-surface temperature anomaly did aid the development of the vortex, then it is not surprising that numerical predictions made without the anomaly were unsuccessful. So, in order to test the hypothesis that the anomaly was important, two predictions were made, one with and one without the warm anomaly. Preliminary results from this experiment have been reported, briefly, in Kershaw (1985b). This account contains a more detailed description and a fuller discussion of the results.

2. EXPERIMENTAL DETAILS

A global model of the atmospheric circulation was used for these experiments. It has a horizontal resolution of 2 degrees of latitude and 3 degrees of longitude. It has 11 layers, and the vertical coordinate is sigma (pressure normalised by surface pressure). It contains parametrizations of physical processes, including convection, radiation, large-scale precipitation, and turbulent mixing in the boundary layer. A complete description may be found in Slingo (1985). The model is not normally used for numerical weather prediction. Its main use is in the study of the general circulation and climate change (e.g. Cunnington and Rowntree 1986).

The initial state of the atmosphere was identical in both predictions. Both started from an analysis for 12 GMT on 11

June 1979. The (Level IIIb) analysis was made by the European Centre for Medium Range Weather Forecasts (ECMWF) using observations specially collected for the Global Weather Experiment (Lorenc 1981). The same analysis was used for the original study of this case reported in Krishnamurti et al. (1983a). Horizontal and vertical interpolation was carried out from the grid of the European Centre's model to the grid of the model used for the predictions. No special initialisation procedure was used after the analysis or the interpolation.

The sea-surface temperatures were kept fixed for the 8 days of each prediction. Over most of the ocean both predictions used the same surface temperatures, long-term climatological averages appropriate for the time of year. The control experiment also used these climatological temperatures for the eastern Arabian Sea (Figure 1a). The anomaly experiment used temperatures based on the analysis of Seetaramayya and Master (1984) for this region (Figure 1b). Figure 1c shows the difference between the surface temperatures used in the experiments. The maximum warm anomaly was 1.7K. Notice also that the anomaly experiment had a much stronger gradient in surface temperature across the Arabian Sea.

3. RESULTS

During the onset of the south-west monsoon the atmospheric circulation undergoes a considerable change. In the lower troposphere a westerly jet becomes established over the Arabian Sea, and in the upper troposphere an easterly jet forms. The rainfall increases in south-west India and moves northwards along the west coast of the peninsula. In June 1979 these changes occurred more rapidly and somewhat later than is usual (Pearce and Mohanty 1984). Figure 2a shows the analysed wind field at the 850-mb level, at 12 GMT on 11 June. At this stage the Somali Jet had not yet fully developed. It had a maximum speed of $14ms^{-1}$ a few degrees to the east of the Somali Peninsula. The main branch of the monsoon flow curved south-eastwards from the Jet towards another area of strong winds south of Sri Lanka. By 12 GMT on 15 June the Somali Jet had strengthened and extended eastwards (Fig. 2b). The onset vortex had formed on its northern flank, close to the Indian coast, and south-westerly winds were affecting the southern peninsula. By 12 GMT on 19 June the vortex had strengthened and had moved first north then west. It lay just a few degrees to the east of the Arabian Peninsula (Fig.2c). The Jet had strengthened further and moved northwards, and the strong westerly winds were affecting the entire west coast of the peninsula.

In the control experiment the Jet does not extend eastwards quickly enough. Neither does it attain sufficient strength. By day 4 of the prediction (12 GMT 15 June) the $15ms^{-1}$ isotach has not reached southern India (see Fig. 3a). A trough has formed on the north-eastern edge of the Jet, but no vortex has formed. By day 8 (12 GMT 19 June) a weak vortex has formed but it remains stationary (Fig. 3b). The Jet has attained a maximum speed of only $24ms^{-1}$, compared with the analysed speed of $29ms^{-1}$. The strong westerly winds are still only affecting the southern part of the peninsula. Thus the control prediction fails to capture the full intensity of the changes that occurred during the onset of the monsoon.

The anomaly experiment produces a much better prediction of these changes. By day 4 (Fig. 4a) the Jet has extended further eastwards and the vortex has already formed. By day 8 (Fig. 4b) the vortex has strengthened and moved north-westwards. The Jet has attained a maximum speed of $29ms^{-1}$, identical to the observed maximum speed, and the entire west coast of the peninsula is under the influence of the strong winds. The prediction is not perfect, but it is very good for an 8-day forecast. Note, however, the following errors. The area of the Jet is too extensive. The centre of the vortex is not far enough north or west. The orientation of the Jet is westerly in the prediction but south-westerly in the analysis. The westerly flow into the Bay of Bengal is too weak. Nevertheless, in several

respects this is the best prediction for this case study published so far. In particular, it is a very good forecast of the formation of the onset vortex and the increase in kinetic energy over the Arabian Sea (see Fig. 5). The kinetic energy increases more in the anomaly experiment than in the control experiment. The increase in the anomaly experiment is similar to the observed increase. However, over the last four days of the experiment the predicted increase actually exceeds the observed increase.

An increase in kinetic energy also occurred at 200 mb. The analysis on 11 June (Fig. 6a) shows a south-easterly flow over the Arabian Sea. A westerly flow is evident over northern India; this is a southern branch of the sub-tropical jet. By 15 June, the easterly jet had strengthened and acquired a northerly, cross-equatorial, component (Fig. 6b). By 19 June the easterly jet had strengthened further and the jet core was over southern India (Fig. 6c). (This northward movement of the jet core happened between 18 and 19 June. On 18 June the jet core was still over the equator and was stronger than on 19 June.) Over northern India the sub-tropical jet had receded northwards leaving a weak easterly flow. The westerly jet itself was strongly anticyclonic. Both experiments (see Figs. 7 and 8) predict the strengthening of the easterly jet and the increase in cross-equatorial flow. Neither experiment predicts the replacement of the weak westerlies by weak easterlies over northern India. The anomaly

experiment is superior in that it predicts a stronger easterly jet, more like the observed jet (although on 19 June the prediction is a little too strong).

The anomaly experiment also produces a better prediction of precipitation than the control (see Figs. 9,a and b). By the end of the forecast period the anomaly experiment has significant amounts (>20mm day^{-1}) over much of the west coast of the peninsula. In the control experiment the precipitation is still restricted to the southern part of the peninsula. The predicted amounts in the anomaly experiment are comparable with those observed over the west coast of India. (Krishnamurti et al. (1983b) give an analysis of daily rainfall using conventional and satellite data.) It is not clear whether the increased precipitation over the Arabian Sea in the anomaly experiment is correct. The predicted maxima are greater than those estimated by Krishnamurti et al. However, their estimates may be too low. A more recent and more detailed analysis by Martin and Howland (1985) shows rainfall maxima exceeding 300mm day^{-1} during the onset. If this later analysis is correct, then the anomaly experiment does have a more realistic distribution of precipitation over the Arabian Sea than the control.

These results support the initial hypothesis that the sea-surface temperature anomaly was instrumental in the development of the onset vortex. Moreover, the use of more accurate sea-surface temperatures has improved the prediction of other aspects of the onset of the monsoon.

The strengthening of the Somali Jet and the easterly jet, and the northward movement of the rainfall are all predicted more accurately in the anomaly experiment than in the control. This is a very good example of the beneficial impact that the use of observed (rather than climatological) sea-surface temperatures can have on numerical weather prediction for the tropics.

4. MECHANISM OF THE ONSET

(a) Role of surface fluxes

Whilst the result of the experiment is interesting in itself, so is the way in which the sea-surface temperature anomaly produces the change in the prediction. The results increase our understanding of the mechanism of the onset in the model. The most obvious effect of the anomaly is to increase the fluxes of heat and moisture into the atmosphere from the sea. There are three components, sensible heat, net radiation , and latent heat. Time series of the difference in these fluxes averaged over the area of the anomaly are shown in Figure 10. The major changes in the prediction are probably caused, indirectly, by these increased fluxes. Several points about the fluxes are noteworthy. Firstly, the increase in latent-heat flux is much bigger than the other components, but its energy can only be released when precipitation occurs. Secondly, the increases in sensible-

and latent-heat fluxes remain steady for the first few days but increase dramatically thereafter; this suggests that a feedback is occurring. Lastly, the increase in radiative-heat flux remains small and steady throughout; hence radiative effects are probably not important. The increased fluxes warm and moisten the atmosphere. However, these changes in the temperature and moisture structure are too small to produce the large changes in the prediction directly. They are also restricted to the boundary layer, whereas the circulation changes affect the entire troposphere.

The increased fluxes increase the precipitation, and it is probably the increased release of latent heat which causes the circulation changes. Figure 11 shows the time series of the difference in the rate of precipitation (P) averaged over the same area as the fluxes. The difference in the rate of evaporation (E, proportional to latent-heat flux) is plotted on the same graph for comparison. The increase in precipitation is largely convective and it is promoted by the warming and moistening of the atmosphere over the anomaly. Note that the precipitation increase exceeds the evaporation increase, except on day 1. Initially, all the moisture necessary to sustain the increase in precipitation is provided by increased evaporation. The total moisture content of the region is increasing and the moisture-flux convergence is positive too. The difference in evaporation stays near its initial

value during the first three days of the experiment. During this time the precipitation difference is increasing rapidly (by 400%). So although the initial increase in precipitation can be explained by the increase in evaporation alone, the subsequent increase must involve some other mechanism. In fact the precipitation increase is sustained by increased moisture-flux convergence. The difference between the precipitation and evaporation curves in Fig. 11 is a measure of this flux convergence (neglecting the small increase in moisture content). Associated with the initial rise in precipitation there is an increase in latent-heat release. Some of this warms the atmosphere but most is compensated by increased adiabatic cooling due to ascent. The increased ascent (Fig. 12) causes convergence of mass at low levels (Fig. 13) and divergence of mass at high levels. Associated with the mass convergence is convergence of moisture flux. This enhances the moisture supply and promotes increasing precipitation, completing the feedback loop. The same mechanism is operating from days 5 to 7; the moisture-flux convergence (P-E) continues to grow throughout this period. However, another mechanism is acting to increase the precipitation. From day 4 onwards the surface fluxes (and in particular the evaporation) are increasing because the wind speed is increasing (Fig. 14). So part of the increase in P is being forced by the increase in E. It remains only to show that the precipitation is causing the increase in wind speeds and another feedback loop has been identified.

(b) Role of precipitation

The simple model developed by GILL (1980) is a useful aid to understanding the dynamical effects of precipitation. It assumes a simple baroclinic structure with maximum heating and vertical velocity, and one reversal of winds, in mid-troposphere. An example is shown in Fig. 15. The contour encloses the imposed heating region and the arrows show the equilibrium response of the low-level wind field. (Note that the upper-level response is obtained by reversing the arrows.) With the particular value of the frictional dissipation parameter used in this example, equilibrium is achieved in less than one day. The solution is obtained analytically using equations which have been linearised about a basic state at rest. It shows that the circulation responds to the heating by generating a strong westerly flow into the heating zone and a cyclonic circulation to the north-west. Weak easterlies are induced to the south and east. The forcing and the response in the numerical experiment show the same pattern. Figure 16 shows the difference fields at 5 days (12 GMT 16 June) for the precipitation and the wind at 850mb. The similarity between Figures 16 and 15 suggests that the circulation change is induced by the heating associated with the precipitation. The difference fields at day 8 (12 GMT 19 June) are shown in Fig. 17. By this time the cyclonic anomaly has started to

move northwards and a prominent maximum has appeared in the precipitation field in the south-west quadrant of the depression. Even after eight days the circulation anomaly is largely restricted to the Arabian Sea, and it still looks like Fig. 15 , even though its magnitude is such that non-linear effects might be expected to be important. Thus the linear model gives the link which completes the second feedback loop identified above; the latent-heat release generates the circulation changes and the increased winds generate the increases in the fluxes. Fig. 18 summarizes the two feedback loops, 1 involving the moisture-flux convergence and 2 involving the surface fluxes. The diagnostics presented so far show that these two mechanisms are important; other mechanisms could also be operating. In particular, instabilities might be aiding the formation of the onset vortex. This problem is discussed in sub-sections 4d and 4e.

(c) Non-linear effects

A more detailed comparison of the predicted anomalies with the results from the linear model reveals some interesting differences. At 850mb, the linear model represents the effect of precipitation in the prediction model quite well, but the momentum balance in the prediction model is not linear. The horizontal advection terms at 850mb are just as large as the other terms in the momentum equation, but they

do not alter the nature of the response (in agreement with the findings of Gill and Phlips (1986)). The vertical structure of the response in the prediction model is similar to that assumed in the linear model; for example, the cross-section of the vertical velocity taken through the centre of the circulation anomaly (Fig. 19) shows a single peak in mid-troposphere. Also, the circulation difference at 200mb (Fig. 20) shows anticyclonic flow above the low-level cyclone, as predicted by the linear model. Note, however, that the high-level flow is not simply a reversal of the low-level flow. The high-level circulation anomaly extends into the Southern Hemisphere. The strongest easterly flow is to the south of the precipitation anomaly, rather than immediately above it. Also the horizontal scale of the anomaly is bigger, extending from the Red Sea to the Bay of Bengal. These factors indicate that non-linear effects are more important at this level. To some extent the advective effects of the north-easterly flow in the control experiment explain this response. A similar response is seen in Gill's model when a non-zero mean flow is imposed (Phlips and Gill 1986). The high-level flow is strongly divergent, whereas the low-level flow is convergent; moreover, the maxima are located differently. At 850mb the major anomalous convergence centre is around 10 degrees North, 70 degrees East (Fig. 21a), in the south-east quadrant of the low-level circulation anomaly (Fig. 17b). At 200mb the major centre of anomalous divergence is north-west of this (Fig. 21b),

associated with the maximum rainfall anomaly in the south-west quadrant (Fig. 17a,b). As the divergence field may be regarded as forcing the vorticity at each level, this difference in location may explain the greater westward extent of the circulation anomaly at 200mb.

Further clarification of the difference between the response at high and low levels is provided by the non-divergent and irrotational components of the circulation anomaly. At 850mb (Fig. 22) the maximum irrotational wind is $5ms^{-1}$, 20% of the non-divergent maximum. At 200mb (Fig. 23) the irrotational flow is relatively stronger ($8ms^{-1}$), more than 50% of the non-divergent component ($14ms^{-1}$). The non-divergent component (Fig. 23a) shows two anticyclonic centres, one over the Arabian Peninsula and the other to the south-east. The feature over Arabia agrees with the expected response of the linear model to the heating in the south-west quadrant of the depression. This is only generated in the last few days of the experiment. The southernmost high is generated on day 1 and moves south-eastwards as the integration progresses. This initial circulation anomaly at 200mb is well predicted by the linear model. But after a few days the detailed development diverges from the linear prediction. So the linear model explains the circulation anomaly at low levels better than that at high levels. Sardeshmukh and Hoskins (1985) came to the same conclusion in their study of the 1982-83 El Nino. Incorporating a non-zero mean wind in the linear model helps

to explain some of the non-linear effects observed. However there are still some details which are not explained. Thus the experiment is a useful demonstration of the potential and limitations of the linear model.

(d) Role of barotropic processes

The discussion so far has implied that the formation of the onset vortex is forced by latent-heat release over the Arabian Sea. However, previous research has suggested that barotropic instability was important in the formation of this vortex (Krishnamurti et al. 1981). Does the same mechanism operate in the numerical model? To investigate this the diagnostic

$$\underset{\sim}{E}=(v'^2-u'^2,-u'v')$$

is used. u and v are the westerly and southerly components of the wind, and ' denotes departure from a time mean ($\overline{\ }$). Hoskins et al. (1983) give details of the applications of $\underset{\sim}{E}$ and the approximations involved in using it. $\underset{\sim}{E}$ enables the interaction between the time-mean flow and the transient eddies to be quantified. For example, convergence of $\underset{\sim}{E}$ implies easterly forcing of the time-mean flow by the eddies. The quantity

$$\overline{u}\,\overline{\underset{\sim}{\nabla}.\underset{\sim}{E}}$$

represents the exchange from the kinetic energy of the eddies to kinetic energy of the mean flow. (More precisely, it represents the local contribution to this barotropic exchange). $\overline{\underset{\sim}{E}}$ and the zonal component of the mean flow for the ECMWF analyses are shown in Fig. 24a. The averaging period is the 8 days of this study. Note that $\overline{\underset{\sim}{E}}$ has a large magnitude on the northern flank of the jet and that the vectors point south-west and converge where $\overline{\pi}$ is positive. In Figure 24b, $\overline{u}\,\overline{\underset{\sim}{\nabla}.\underset{\sim}{E}}$ is strongly negative when averaged over the Arabian Sea, implying that the transient eddies grew at the expense of the mean flow.

Krishnamurti et al. (1981) showed that the necessary condition for barotropic instability was satisfied in this region at this time. They also diagnosed that energy was transferred from the zonal flow to the vortex. At first sight this $\underset{\sim}{E}$-vector analysis confirms that diagnosis. However, there are several difficulties over diagnosing barotropic processes near an extending jet. The basic flow is zonally varying, so the theory of instability of a zonally uniform flow is of doubtful relevance. Although the $\underset{\sim}{E}$-vector approach eliminates this problem it raises another. It is difficult to define eddies in a way which isolates them from the jet. The use here of deviations from a time mean is only partially successful. Because the jet is extending, $\overline{u'^2}$ is large in the jet exit, so $\overline{\underset{\sim}{E}}$ has a substantial component towards the west. It would have even

if no vortex formed. Thus the barotropic energy conversion diagnosed here is, in part, an artefact of the definition of eddies. Furthermore, the existence a barotropic energy conversion does not necessarily imply that barotropic instability is present. Nevertheless, the $\underset{\sim}{E}$-vector analysis presented here is consistent with the growth of the onset vortex by barotropic processes.

The same diagnostics are shown for the control prediction in Fig. 25. The arrows are drawn to the same scale as in Fig. 24 but they are much smaller. The energy conversion term in Fig. 25b is only weakly negative, indicating that barotropic processes are not very effective in the control experiment. This is consistent with the development of the onset vortex being underestimated in that prediction. For the anomaly prediction (Fig. 26) the $\underset{\sim}{E}$ vectors are more like those diagnosed from the analyses (Fig. 24), and the energy conversion term is more negative. These results are consistent with barotropic processes being important in the growth of the vortex in the model, but further research is needed to verify this.

(e) Role of baroclinic instability

The relative importance of barotropic and baroclinic processes in the formation of monsoon depressions has attracted much attention (Moorthi and Arakawa 1985; Lindzen et al. 1983; Das 1986). It is of interest, therefore, to

ask whether baroclinic instability is also important in the formation of the onset vortex. To shed some light on this a $\underset{\sim}{Q}$-vector analysis has been performed. $\underset{\sim}{Q}$ is defined as

$$\left(\frac{-g}{\theta_s}\frac{\partial \underset{\sim}{V}_g}{\partial x}\cdot\nabla\theta, \frac{-g}{\theta_s}\frac{\partial \underset{\sim}{V}_g}{\partial y}\cdot\nabla\theta\right)$$

where $\underset{\sim}{V}_g$ is the geostrophic wind, θ is the temperature at the same level, and θ_s is an arbitrary reference temperature. $\underset{\sim}{Q}$ is a convenient diagnostic because it only requires data for a single isobaric level and it only involves horizontal derivatives. It can be used to diagnose vertical velocity; convergence of $\underset{\sim}{Q}$ implies ascent and divergence implies descent. (This assumes that the quasi-geostrophic approximation holds and that f is constant. Hoskins et al. (1978) give details.) This diagnosis reveals areas of ascent and descent which are forced dynamically, by the geostrophic flow, rather than by the release of latent heat. Figure 27 shows the difference in $\underset{\sim}{Q}$ and its divergence between the two predictions at 12 GMT 18 June. This chart is for 500mb but similar features can be seen at other levels, and at other times. In the region just west of India where the precipitation anomaly for the day beginning 12 GMT 18 June (Fig. 17a) has a maximum, $\underset{\sim}{Q}$ is divergent, implying descent. But this is the region of maximum mass convergence at 850mb which we have suggested is the primary forcing region for the development of the onset vortex. It is also a

region of positive temperature anomaly (not shown). If baroclinic instability were aiding this development then dynamically forced ascent would be found in this region. As it is not, such instability is probably not important in the development of the vortex.

However, $\underset{\sim}{Q}$ is convergent near 15°N 60°E, and so ascent is being forced dynamically in the south-west quadrant of the circulation anomaly, where a secondary maximum in anomalous precipitation occurs (see Fig. 17). Rainfall maxima are frequently observed in the south-west quadrant of monsoon depressions and Douglas (1985) has suggested that ascent (and hence precipitation) is forced dynamically in that quadrant. The results from this study suggest that this is also true for the onset vortex. The occurrence of this feature might explain the north-westward movement of the vortex, for the linear model suggests that heating in such a region will force cyclonic vorticity to the north-west. This suggestion is, however, purely speculative.

5. IMPORTANCE OF SEA-SURFACE TEMPERATURE ANOMALIES

In this case study it was important to specify the correct sea-surface temperatures to get a good prediction of developments in the tropics. When else might this be important? Sea-surface temperature anomalies can probably contribute to the development of severe tropical storms, for it is well known that these storms develop preferentially

over warmer waters. In fact similar feedback mechanisms to the two identified in section 4 are important in their development (Gray 1982). An important factor is the occurrence of strong winds over the anomaly which amplify the response. Monsoon disturbances will therefore be particularly sensitive to sea-surface temperature anomalies, because they develop near the low-level jet. The normal gradient of sea-surface temperature in the Arabian Sea will also amplify the impact of anomalies in the east, because the prevailing winds flow up the gradient, from cooler to warmer seas. So it seems likely that the onset of the monsoon in other years will be sensitive to such anomalies. In particular, in years when the onset is late warmer than normal temperatures might be expected in the Arabian Sea because of the extra solar heating available before the cloudiness increases at onset. The delay in the cooling associated with the onset will also help. The onset of the monsoon was also late in 1983. During this year the sea-surface temperature anomaly in the Arabian Sea was +2K just prior to the onset. This suggests that the onset in 1983 would be a good case on which to perform a prediction experiment similar to the one reported here. This preliminary research suggests that the following phenomena may be correlated and should be the subject of further study: Late onset of the monsoon, warm anomaly in the Arabian Sea, sudden onset of the monsoon (rapid northward

progress), and occurrence of an onset vortex. Some of these relationships may have predictive value.

6. PROBLEMS

The cooling of the Arabian Sea during the onset casts some doubt on the results reported here. For although the sea-surface temperatures imposed in the anomaly experiment are realistic for 11 June, it has been suggested that they are too warm for 19 June. To some extent this is true; the model is being forced by too strong an anomaly. This may explain why the growth of kinetic energy over the Arabian Sea is overestimated in the last half of the anomaly experiment (Fig. 5). However, the error is not very great; even on 19 June ships in the eastern Arabian Sea were reporting temperatures in excess of 303K. The cooling of the Arabian Sea starts in the west and south and then spreads northwards and eastwards. The cooling in the northern part occurred only after the period of this study (see Krishnamurti (1985) Fig. 9d). The warm anomaly remained in the north and the anomaly imposed in the model is an underestimate in this region. So, although the imposed surface temperatures are too warm in the south they are too cold in the north. These errors will tend to act in opposition. In fact, incorporation of this northern anomaly might even improve the prediction by inducing northward movement of the jet and the vortex.

7. CONCLUSION

An example of a forecast for the tropics has been presented in which a sea-surface temperature anomaly had a substantial impact; such anomalies will also be important in other cases. Several major weather forecasting centres already use analysed sea temperatures in their operational prediction models; this study confirms that it is important to do so. The main conclusion of this study is that the warm anomaly in the Arabian Sea did affect the onset of the monsoon. It increased the rate of generation of kinetic energy, speeding up the onset and causing rapid northward progression of the monsoon. It also promoted the formation of the onset vortex, by enhancing the release of latent heat and perhaps by promoting barotropic instability. Latent-heat release in the Arabian Sea played a very important part in the mechanism of the onset in the prediction model. It had a crucial role in the two feedback loops which were identified as dominant, one involving moisture-flux convergence, the other involving the surface fluxes. The same mechanisms probably operated in the real atmosphere, but without more observations (especially of surface fluxes) this cannot be verified. Various diagnostic techniques have shed considerable light on the workings of the prediction model in this case. Firstly, Gill's linear model helped to identify the crucial connection between the

release of latent heat and the response of the circulation. Secondly, the diagnostics $\underset{\sim}{E}$ and $\underset{\sim}{Q}$, developed by Hoskins, helped to clarify the roles of barotropic processes and baroclinic instability in the formation of the onset vortex.

ACKNOWLEDGMENTS

I would like to thank R.A. Bromley, D.J. Carson, H. Cattle, A.E. Gill, B.J. Hoskins, M.E. McIntyre, P.D. Sardeshmukh, and C.A. Wilson for constructive criticism at various stages of this study. I am also grateful to P.J. Phlips for providing Fig. 15, and to P.V. Harker and P.A. Whitfield for their help with the computing.

REFERENCES

Cunnington, W.M. and Rowntree, P.R. 1986. *Simulations of the Saharan atmosphere - dependence on moisture and albedo.* Quart. J. R. Met. Soc., 112 (in press).

Das, P.K. 1986. Monsoons. WMO, Geneva.

Douglas, M. 1985. Monsoon depression structure and rainfall from Summer MONEX data. GARP Special Report No. 44, ICSU/WMO, Geneva, section V, 35-40.

Gill, A.E. 1980. Some simple solutions for heat-induced tropical circulation. Quart. J. R. Met. Soc., 106, 447-462.

Gill, A.E. and Phlips, P.J. 1986. Non-linear effects on heat-induced circulation of the tropical atmosphere. Quart. J. R. Met. Soc., 112, 69-91.

Gray, W.M. 1982. Cyclone genesis and intensification. Bengtsson, L. and Lighthill J., editors. Intense atmospheric vortices. Springer-Verlage, Berlin, 3-20.

Haskins, B.J., Draghici, I. and Davies, H.C. 1978. A new look at the omega equation. Quart. J. R. Met. Soc., 104, 31-38.

Hoskins, B.J., James, I.N. and White, G.H. 1983. The shape, propagation and mean-flow interaction of large-scale weather systems. J. Atmos. Sci., 40, 1595-1612.

Kershaw, R. 1985a. Numerical experimentation at the U.K. Meteorological Office. GARP Special Report No. 44, ICSU/WMO, Geneva, section IV, 60-77.

Kershaw, R. 1985b. Onset of the south-west monsoon and sea-surface temperature anomalies in the Arabian Sea. Nature, 315, 561-563.

Krishnamurti, T.N. 1985. Summer Monsoon Experiment - a revue. Mon. Wea. Rev., 113, 1590-1626.

Krishnamurti, T.N., Pasch, R. and Kitade, T. 1983a. WGNE forecast comparison experiments. Numerical experimentation programme, Report No. 6, WCRP, ICSU/WMO, Geneva, 73-104.

Krishnamurti, T.N., Ardanuy, P., Ramanathan, Y. and Pasch, R. 1981. On the onset vortex of the summer monsoon. Mon. Wea. Rev., 109, 344-363.

Krishnamurti, T.N., Cocke, S., Pasch, R. and Low-Nam, S. 1983b. Precipitation estimates for raingauge and satellite observations. Florida State University Report No. 83-7, Dept. of Meteorology, Tallahassee.

Krishnamurti, T.N., Ingles, K., Cocke, S., Kitade, T. and Pasch, R. 1984. Details of low latitude medium range numerical weather prediction using a global spectral model. II Effects of orography and physical initialization. J. Met. Soc. Japan, 62, 613-649.

Lindzen, R.S., Farrel, B. and Rosenthal, A.J. 1983. Absolute barotropic instability and monsoon depressions. J. Atmos. Sci., 40, 1178-1184.

Lorenc, A.C. 1981. A global three-dimensional multivariate statistical interpolation scheme. Mon. Wea. Rev., 109, 701-721.

Martin, D.W. and Howland, M.R. 1985. Daily Arabian Sea rainfall during the onset of the 1979 monsoon: a satellite estimate. Pap. Met. Res., 6, 91-100.

Moorthi, S. and Arakawa, A. 1985. Baroclinic instability with cumulus heating. J. Atmos. Sci., 42, 2007-2031.

Pearce, R.P. and Mohanty, U.C. 1984. Onsets of the Asian summer monsoon 1979-82. J. Atmos. Sci., 41, 1620-1639.

Phlips, P.J. and Gill, A.E. 1986. An analytic model of the heat-induced tropical circulation in the presence of a mean wind. Quart. J. R. Met. Soc., 112 (in press).

Sardeshmukh, P.D. and Hoskins, B.J. 1985. Vorticity balances in the tropics during the 1982-83 El Nino - Southern Oscillation event. Quart. J. R. Met. Soc., 111, 261-278.

Seetaramayya, P. and Master, A. 1984. Observed air-sea interface conditions and a monsoon depression during MONEX-79. Arch. Met. Geophys. Biokl., A33, 61-67.

Slingo, A. 1985. Handbook of the Meteorological Office 11-Layer atmospheric general circulation model. Vol. 1: model description. Ed. A. Slingo. Dynamical Climatology Technical Note 29, Meteorological Office, Bracknell.

FIGURE CAPTIONS

Fig. 1 Sea-surface temperature a) for control forecast, b) for anomaly forecast, c) difference (b-a). Units K, contour interval 0.5 K.

Fig. 2 Wind vectors and isotachs at 850 mb from ECMWF FGGE IIIb analysis a) 12 GMT 11 June 1979, b) 12 GMT 15 June 1979, c) 12 GMT 19 June 1979. Units ms^{-1}, contour interval 5 ms^{-1}.

Fig. 3 Wind vectors and isotachs at 850 mb from control forecast a) day 4, 12 GMT 15 June 1979, b) day 8, 12 GMT 19 June 1979. Units ms^{-1}, contour interval 5 ms^{-1}.

Fig. 4 Wind vectors and isotachs at 850 mb from anomaly forecast a) day 4, 12 GMT 15 June 1979, b) day 8, 12 GMT 19 June 1979. Units ms^{-1}, contour interval 5 ms^{-1}.

Fig. 5 Kinetic energy per unit mass at 850 mb, averaged over Arabian Sea (4°S to 20°N, 50°E to 70°E). Full line - ECMWF FGGE IIIb analysis, dashed line - control forecast, crosses - anomaly forecast.

Fig. 6 Wind vectors and isotachs at 200 mb from ECMWF FGGE IIIb analysis a) 12 GMT 11 June 1979, b) 12 GMT 15 June 1979, c) 12 GMT 19 June 1979. Units ms^{-1}, contour interval 10 ms^{-1}.

Fig. 7 Wind vectors and isotachs at 200 mb from control forecast a) day 4, 12 GMT 15 June 1979, b) day 8, 12 GMT 19 June 1979. Units ms^{-1}, contour interval 10 ms^{-1}.

Fig. 8 Wind vectors and isotachs at 200 mb from anomaly forecast a) day 4, 12 GMT 15 June 1979, b) day 8, 12 GMT 19 June 1979. Units ms^{-1}, contour interval 10 ms^{-1}.

Fig. 9 Forecast rate of precipitation, averaged over day ending 12 GMT 19 June 1979 (day 8) a) control, b) anomaly. Units mm day^{-1}, contour interval 20 mm day^{-1}.

Fig. 10 Difference (anomaly - control) in upward flux at surface, averaged over area of sea-surface temperature anomaly (4° N to 20° N, 60° E to 76° E) and over each day of forecast. Solid line - sensible heat, dashed line - latent heat, crosses - net radiation.

Fig. 11 Difference (anomaly - control) in rates of precipitation (full line) and evaporation (dashed line), averaged over area of sea-surface temperature anomaly (4° N to 20° N, 60° E to 76° E) and over each day of forecast.

Fig. 12 Difference (anomaly – control) in vertical velocity at 500 mb (negative upwards), averaged over area of sea-surface temperature anomaly (4°N to 20°N, 60°E to 76°E) at end of each day of forecast.

Fig. 13 Difference (anomaly – control) in divergence at 850 mb, averaged over area of sea-surface temperature anomaly (4°N to 20°N, 60°E to 76°E) at end of each day of forecast.

Fig. 14 Difference (anomaly – control) in wind speed at 850 mb, averaged over area of sea-surface temperature anomaly (4°N to 20°N, 60°E to 76°E) at end of each day of forecast.

Fig. 15 Equilibrium response of low-level wind (shown by arrows) to a region of heating (enclosed by contour) north of equator (y=0) in a linear model. One unit of length is approximately 10 latitude. (After Gill (1980), courtesy of P. J. Phlips)

Fig. 16 Difference charts, anomaly – control forecast at 12 GMT 16 June 1979 (day 5). a) Rate of precipitation averaged over preceeding day. Units mm day^{-1}, contour interval 20 mm day^{-1}. b) Vector wind at 850 mb. Contours show magnitude of difference. Units ms^{-1}, contour interval 5 ms^{-1}.

Fig. 17 Difference charts, anomaly - control forecast at 12 GMT 19 June 1979 (day 8). a) Rate of precipitation averaged over preceeding day. Units mm day^{-1}, contour interval 20 mm day^{-1}. b) Vector wind at 850 mb. Contours show magnitude of difference. Units ms^{-1}, contour interval 5 ms^{-1}.

Fig. 18 Mechanism of onset in model, showing feedback loops 1 and 2 identified in text.

Fig. 19 Cross-section along 67.5° E showing difference (anomaly - control forecast) in vertical velocity (negative upwards) at 12 GMT 16 June 1979 (day 5). Units mb hr^{-1}, contour interval 1 mb hr^{-1}.

Fig. 20 Difference (anomaly - control forecast) in wind vector at 200 mb at 12 GMT 19 June 1979 (day 8). Contours show magnitude of difference. Units ms^{-1}, contour interval 5 ms^{-1}.

Fig. 21 Difference (anomaly - control forecast) in divergence at a) 850 mb, b) 200 mb at 12 GMT 19 June 1979 (day 8). Units 10^{-6} s^{-1}, contour interval 10^{-5} s^{-1}, zero contour omitted.

Fig. 22 Difference (anomaly - control forecast) in a) non-divergent, b) irrotational wind vector at 850 mb at 12 GMT 19 June 1979 (day 8). Contours show magnitude of difference. Units ms^{-1}, contour interval 5 ms^{-1}.

Fig. 23 Difference (anomaly - control forecast) in a) non-divergent, b) irrotational wind vector at 200 mb at 12 GMT 19 June 1979 (day 8). Contours show magnitude of difference. Units ms^{-1}, contour interval 5 ms^{-1}.

Fig. 24 a) $\overline{\underset{\sim}{E}}$ (units $m^2 s^{-2}$) and isotachs of $\overline{u}$ (units ms^{-1}, contour interval 5 ms^{-1}), b) $\overline{u}.\overline{\underset{\sim}{\nabla}.\underset{\sim}{E}}$ (units 10^{-3} $m^2 s^{-3}$, contour interval 0.5 10^{-3} $m^2 s^{-3}$), averaged over 8 days from 12 GMT 12 June 1979 to 12 GMT 19 June 1979, calculated from ECMWF FGGE IIIb analyses at 850 mb.

Fig. 25 a) $\overline{\underset{\sim}{E}}$ (units $m^2 s^{-2}$) and isotachs of $\overline{u}$ (units ms^{-1}, contour interval 5 ms^{-1}), b) $\overline{u}.\overline{\underset{\sim}{\nabla}.\underset{\sim}{E}}$ (units 10^{-3} $m^2 s^{-3}$, contour interval 0.5 10^{-3} $m^2 s^{-3}$), averaged over 8 days from 12 GMT 12 June 1979 to 12 GMT 19 June 1979, calculated from control forecast at 850 mb.

Fig. 26 a) $\overline{\underset{\sim}{E}}$ (units $m^2 s^{-2}$) and isotachs of $\overline{u}$ (units ms^{-1}, contour interval 5 ms^{-1}), b) $\overline{u}.\overline{\underset{\sim}{\nabla}.\underset{\sim}{E}}$ (units 10^{-3} $m^2 s^{-3}$, contour interval 0.5 10^{-3} $m^2 s^{-3}$), averaged over 8 days from 12 GMT 12 June 1979 to 12 GMT 19 June 1979, calculated from anomaly forecast at 850 mb.

Fig. 27 Difference (anomaly - control forecast) in a) $\underset{\sim}{Q}$ (units s^{-3}), b) $\underset{\sim}{\nabla}.\underset{\sim}{Q}$ (units $10^{-18} s^{-3} m^{-1}$; contour interval $5.10^{-18} s^{-3} m^{-1}$) at 500 mb at 12 GMT 19 June 1979 (day 8).

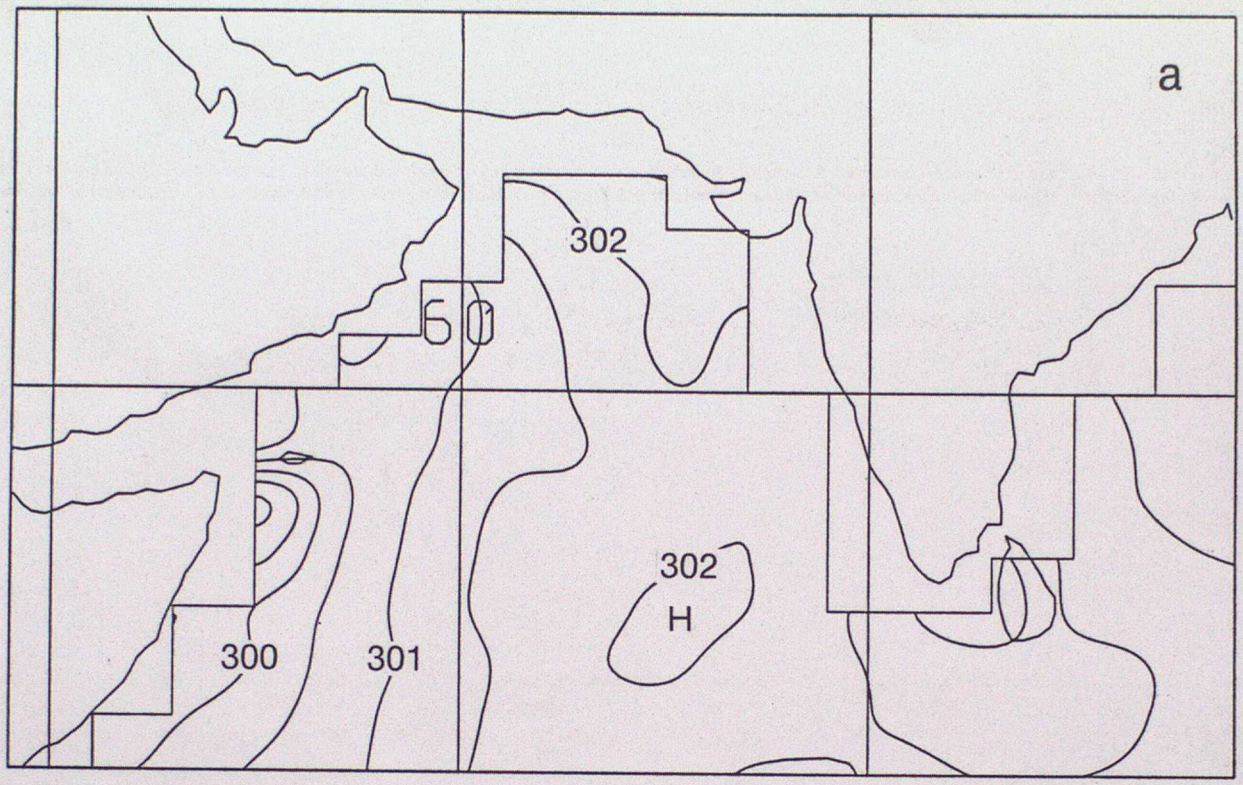

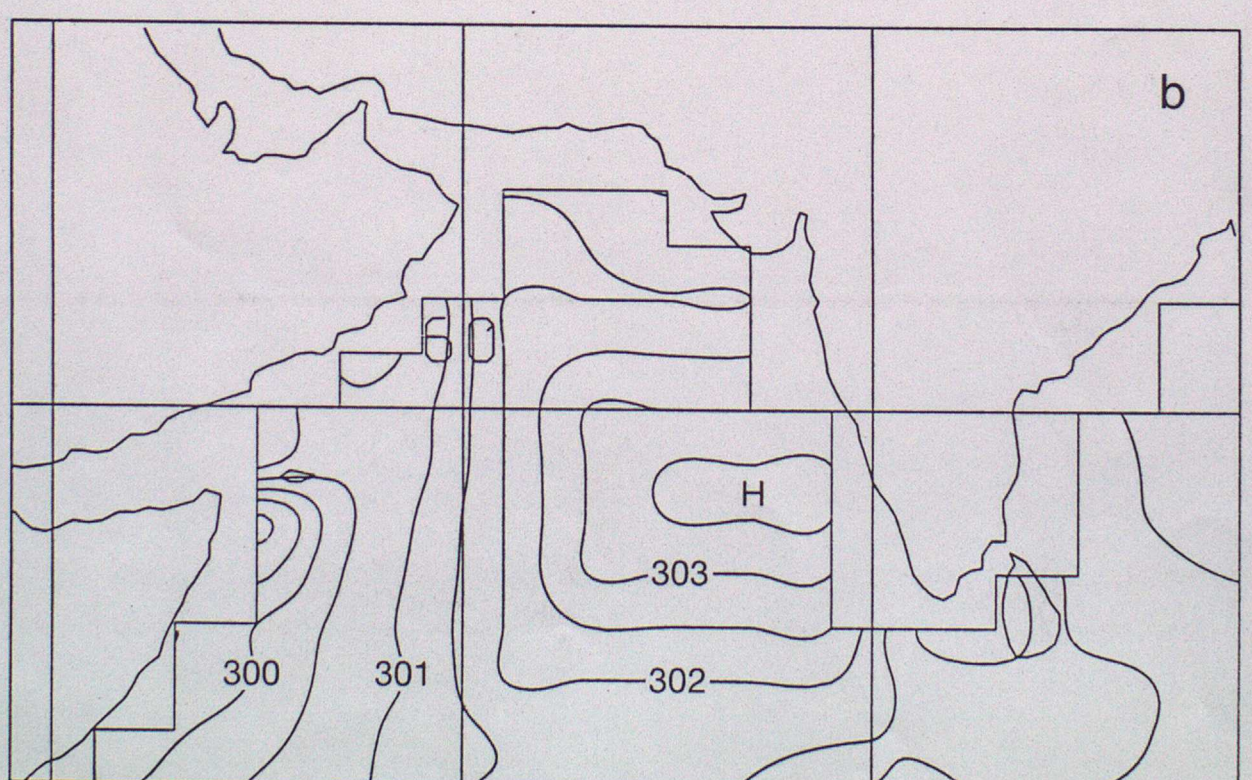

fig. 1 a, b

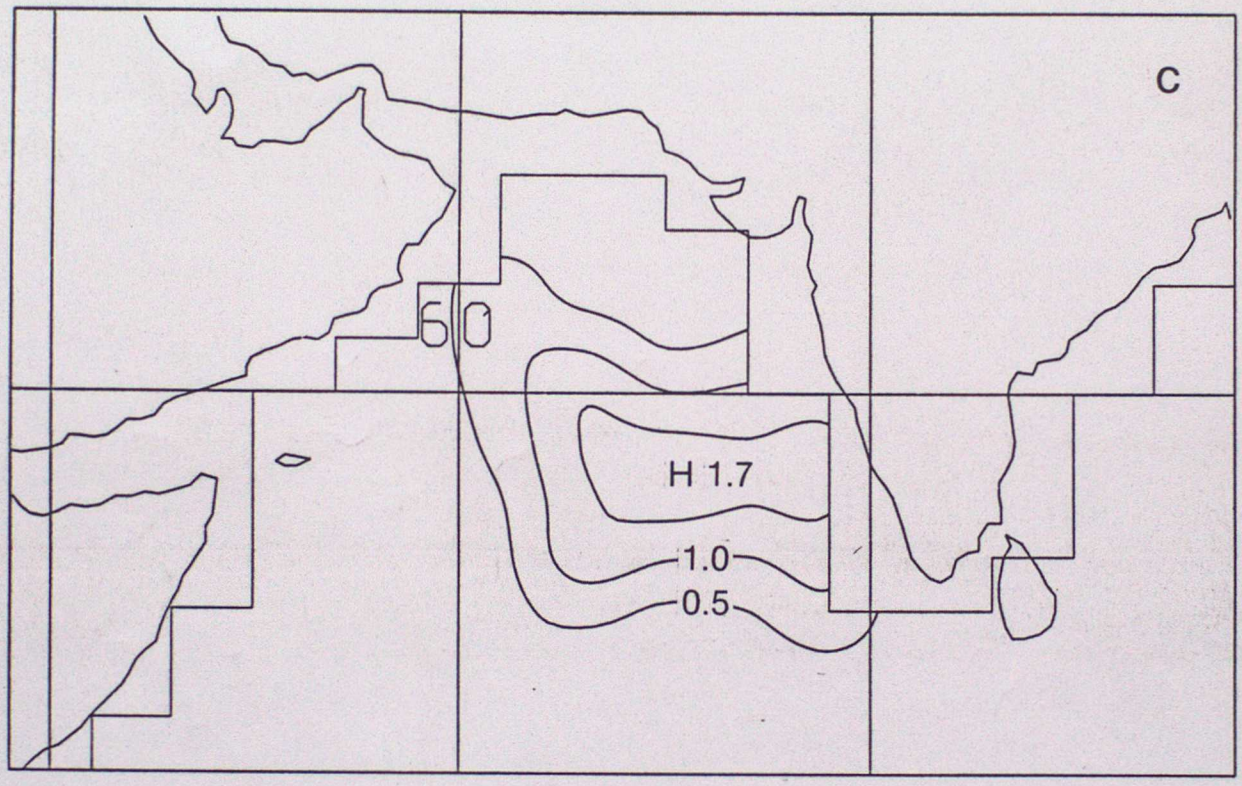

fig. 1c

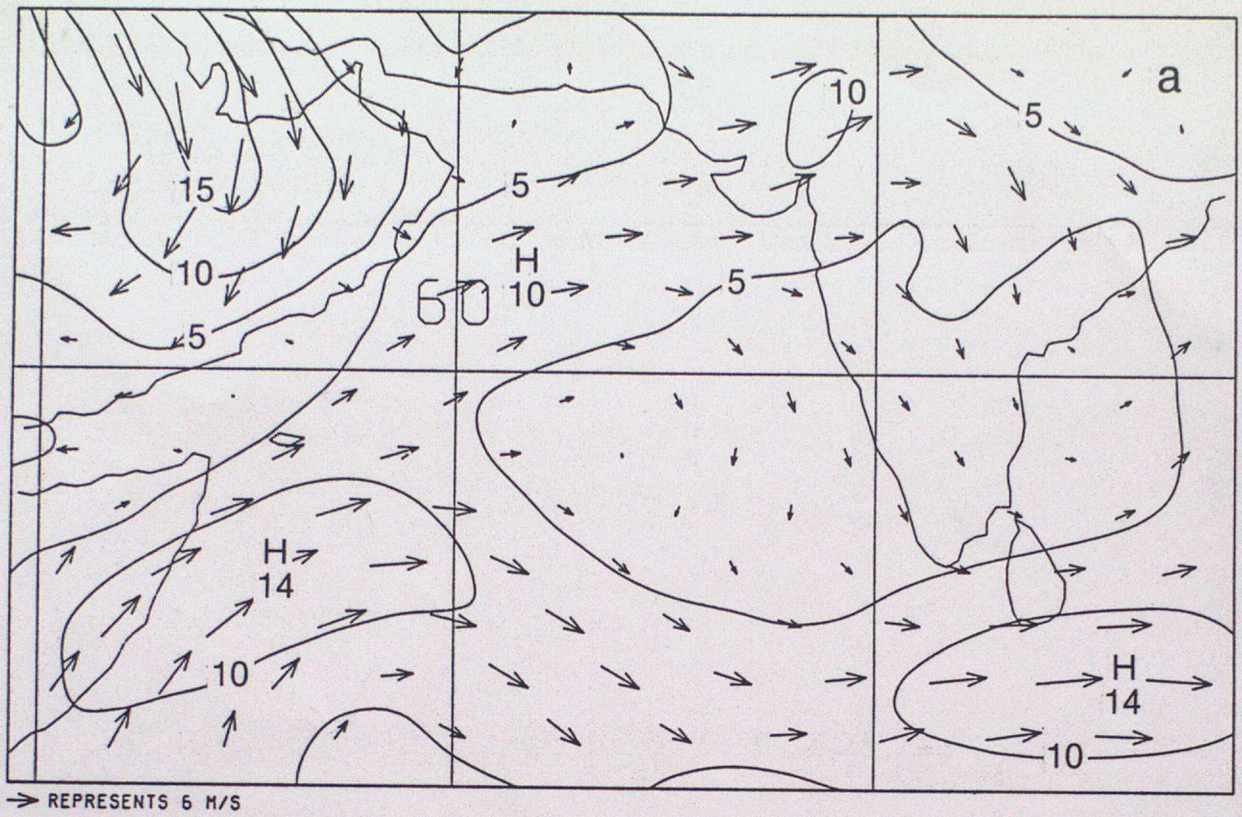
a
10
5
15
5
H
10
60
10
5
H
14
10
H
14
10
REPRESENTS 6 M/S

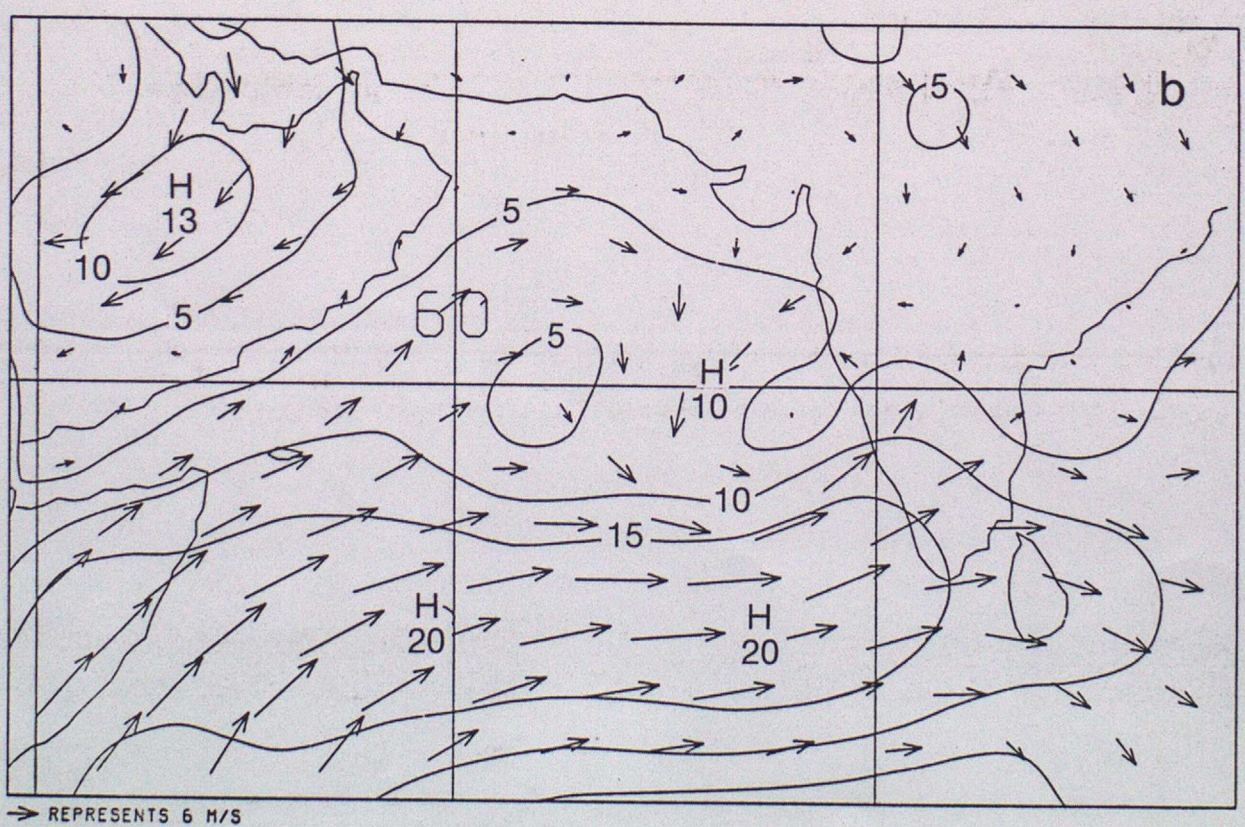
b
5
H
13
10
5
5
60
5
H
10
10
15
H
20
H
20
REPRESENTS 6 M/S

fig. 2a,b

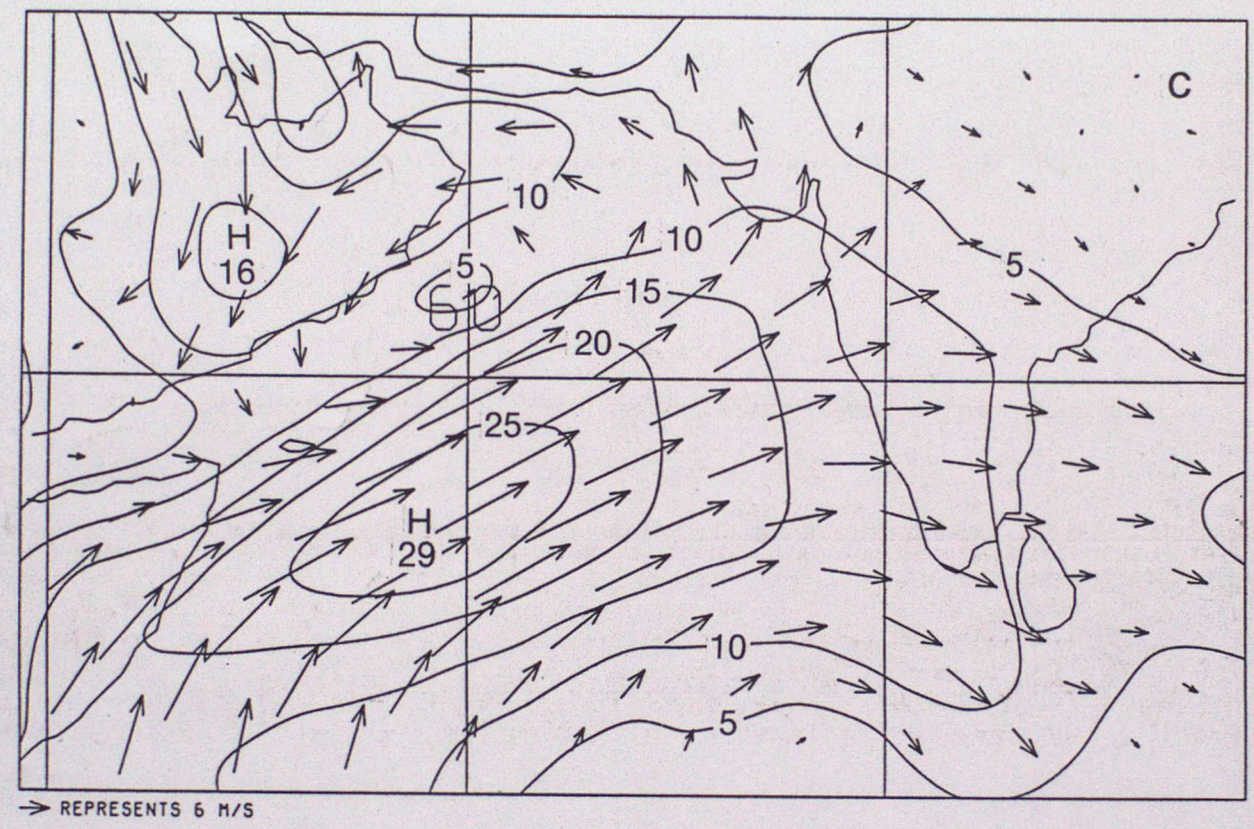

fig. 2c

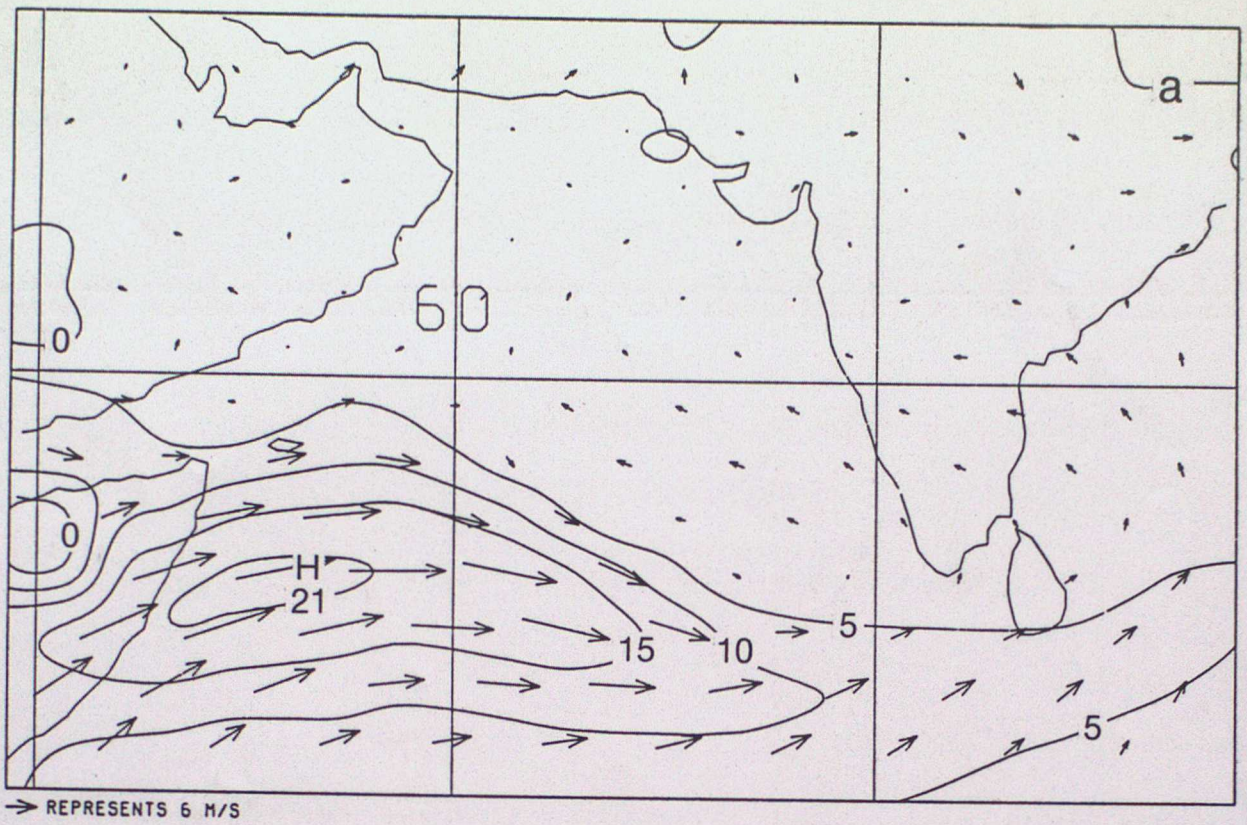
a
60
0
0
H
21
15
10
5
5
REPRESENTS 6 M/S

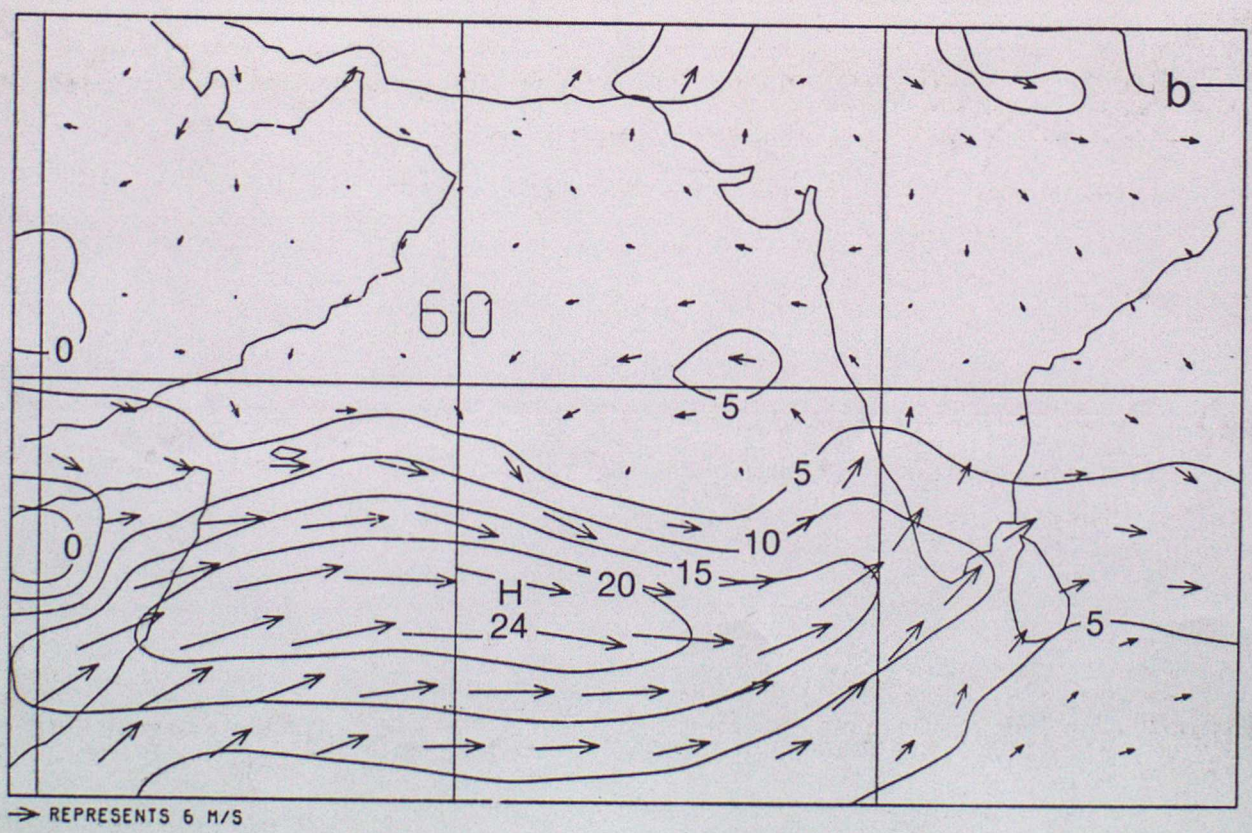
b
60
0
5
5
0
10
15
H
20
24
5
REPRESENTS 6 M/S

fig. 3a,b

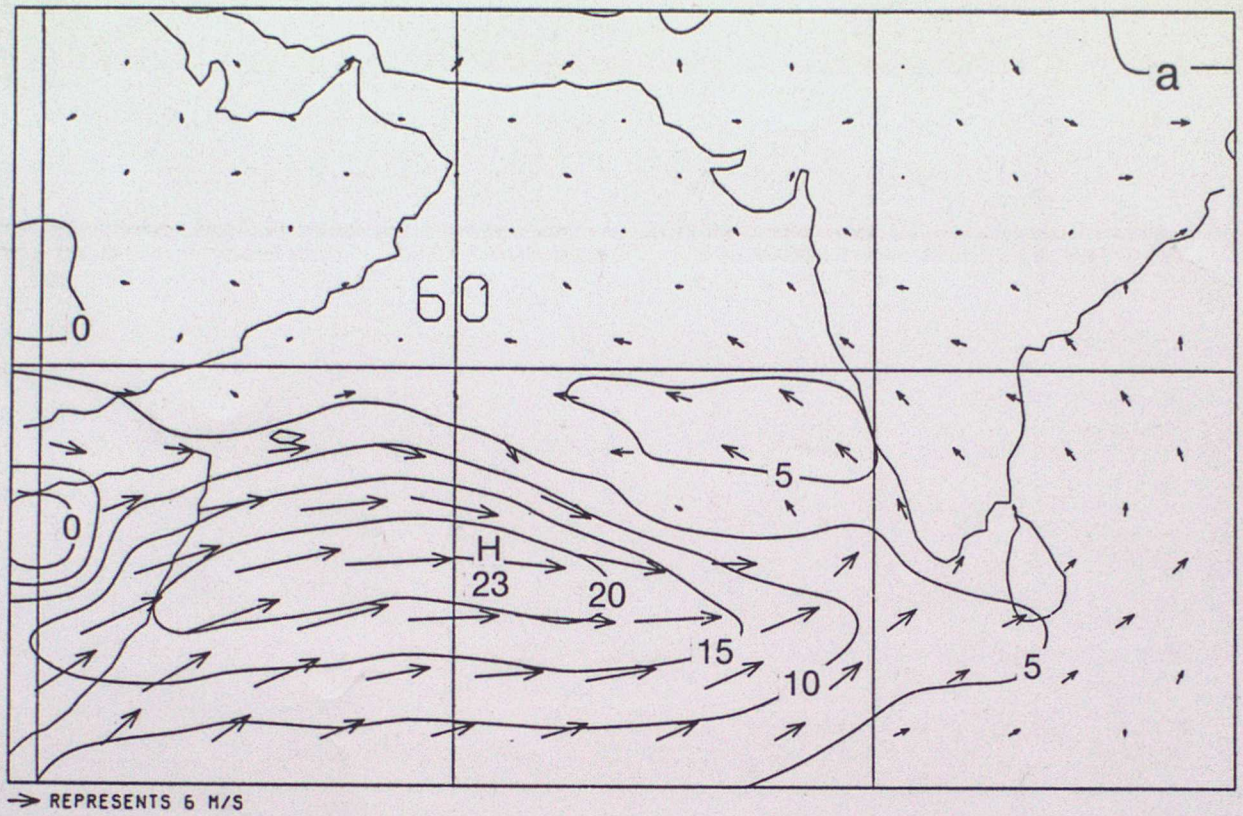
a
60
0
0
5
H
23
20
15
10
5
→ REPRESENTS 6 M/S

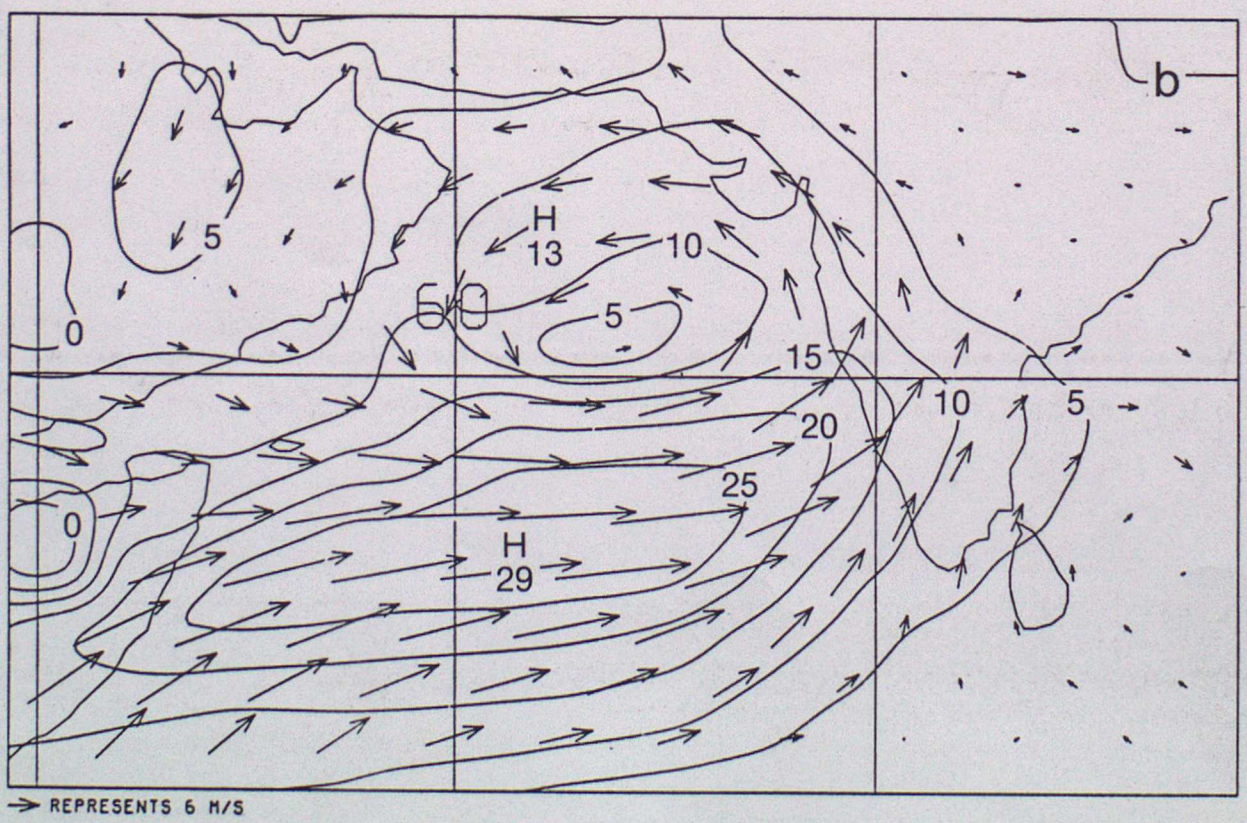
b
5
H
13
10
60
5
0
15
10
5
20
25
0
H
29
→ REPRESENTS 6 M/S

fig. 4 a,b

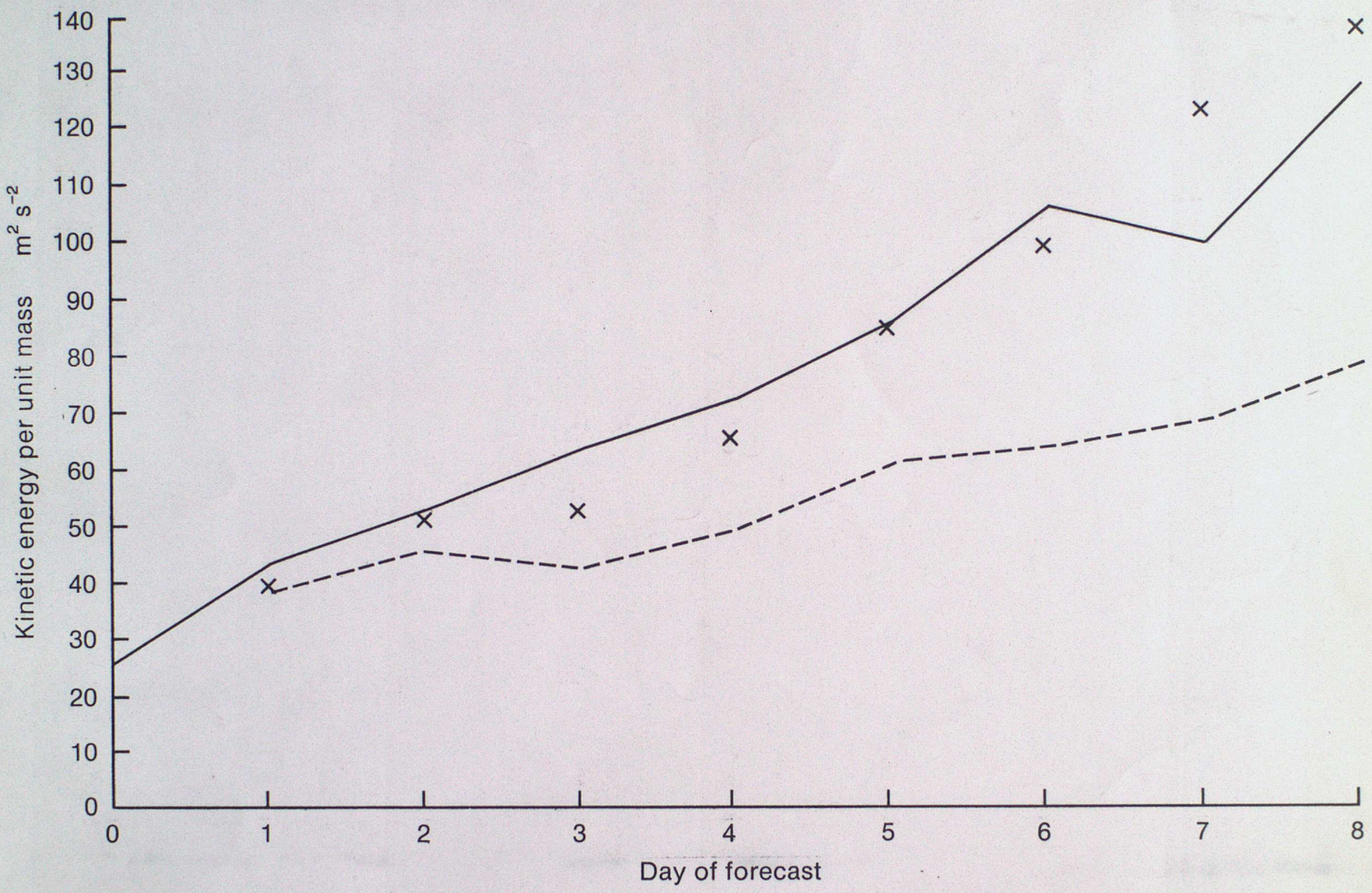
Kinetic energy per unit mass m² s⁻²
140
130
120
110
100
90
80
70
60
50
40
30
20
10
0
0
1
2
3
4
5
6
7
8
Day of forecast

Fig. 5

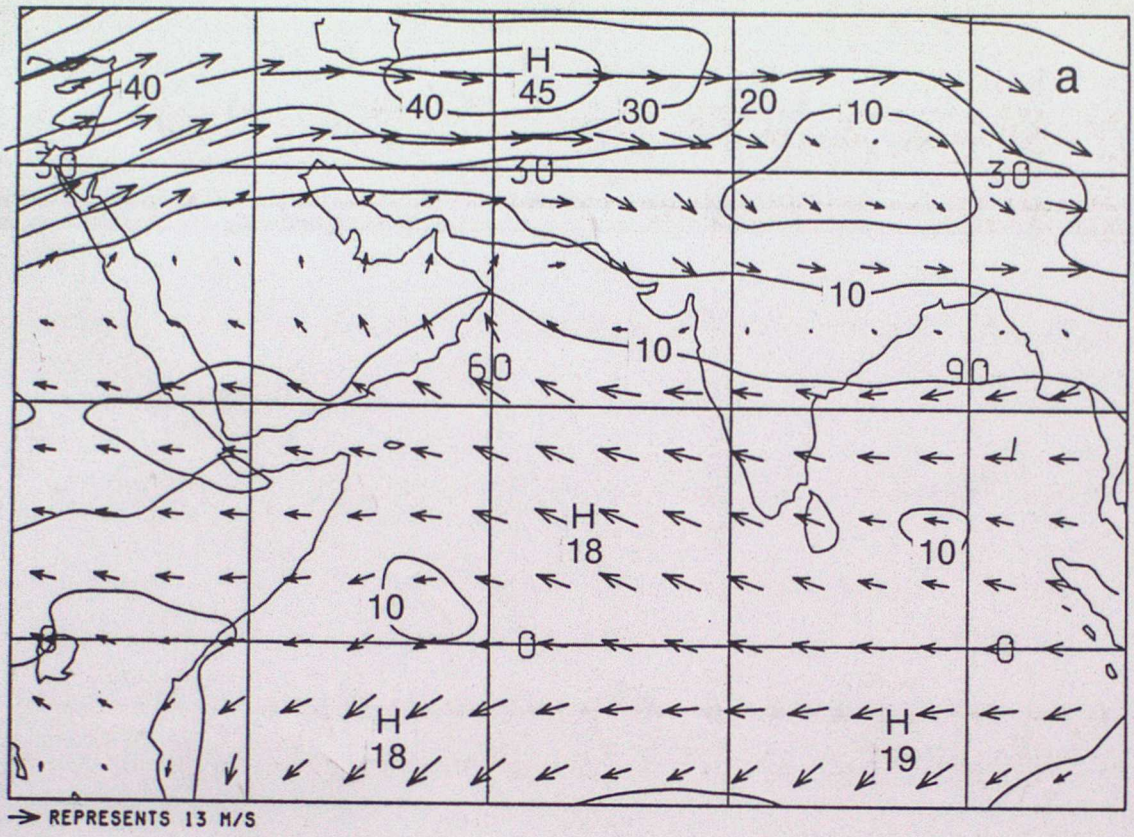
a
H
45
40
40
30
20
10
30
30
30
10
10
60
90
H
18
10
10
0
0
0
H
18
H
19
→ REPRESENTS 13 M/S

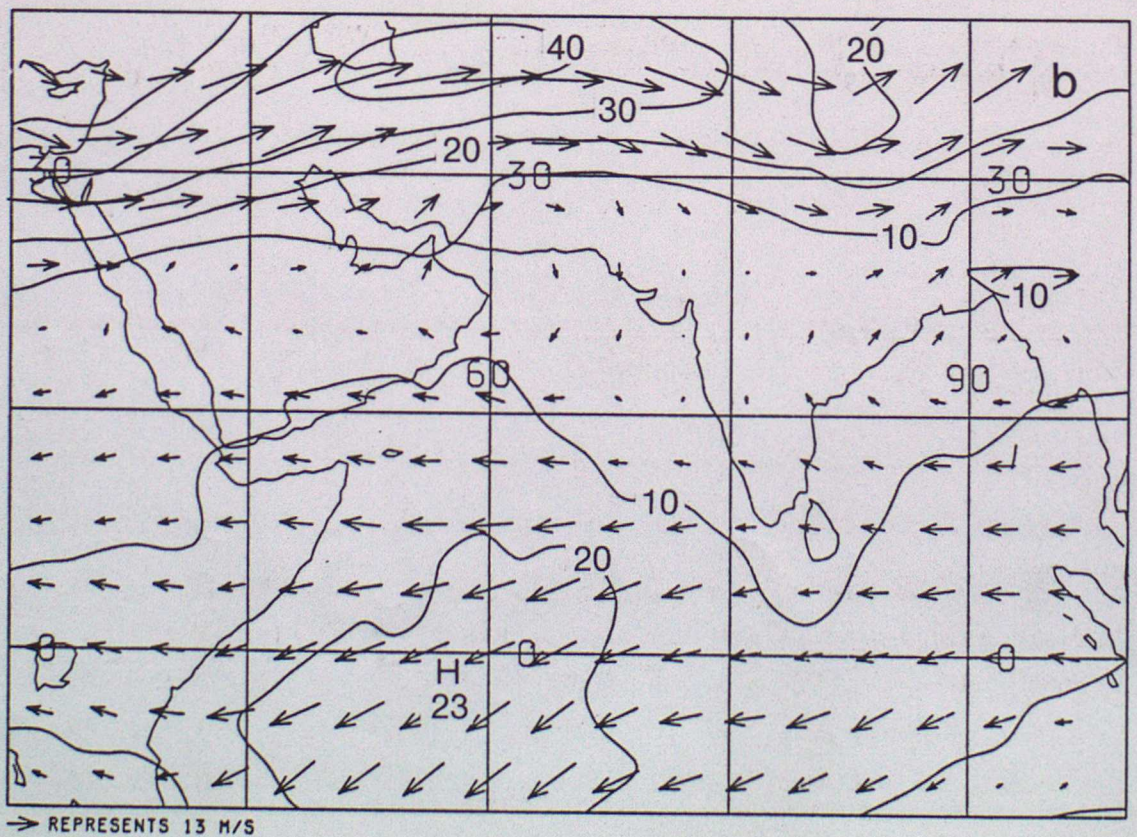
b
40
20
30
20
30
30
10
10
60
90
10
20
0
0
0
H
23
→ REPRESENTS 13 M/S

fig. 6 a,b

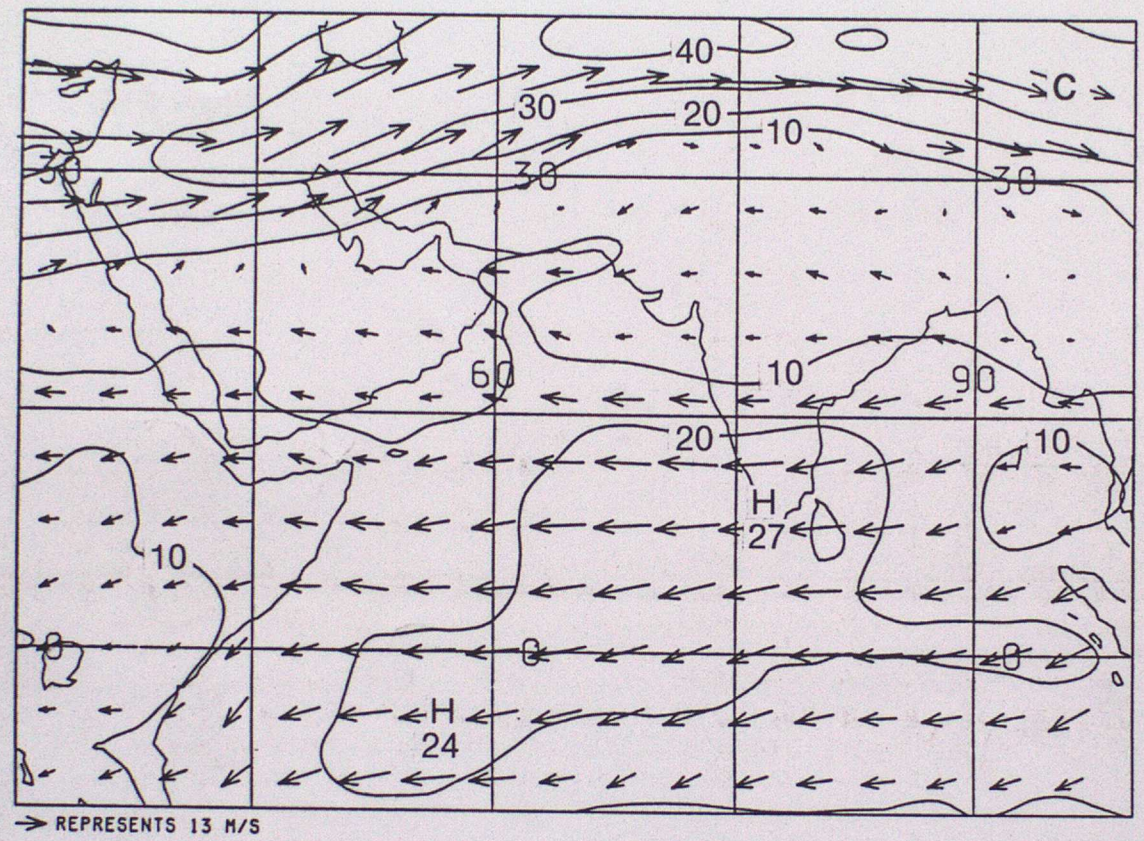
40
30
20
10
C
30
30
30
60
10
90
20
10
H
27
10
0
0
0
H
24
→ REPRESENTS 13 M/S

fig. 6c

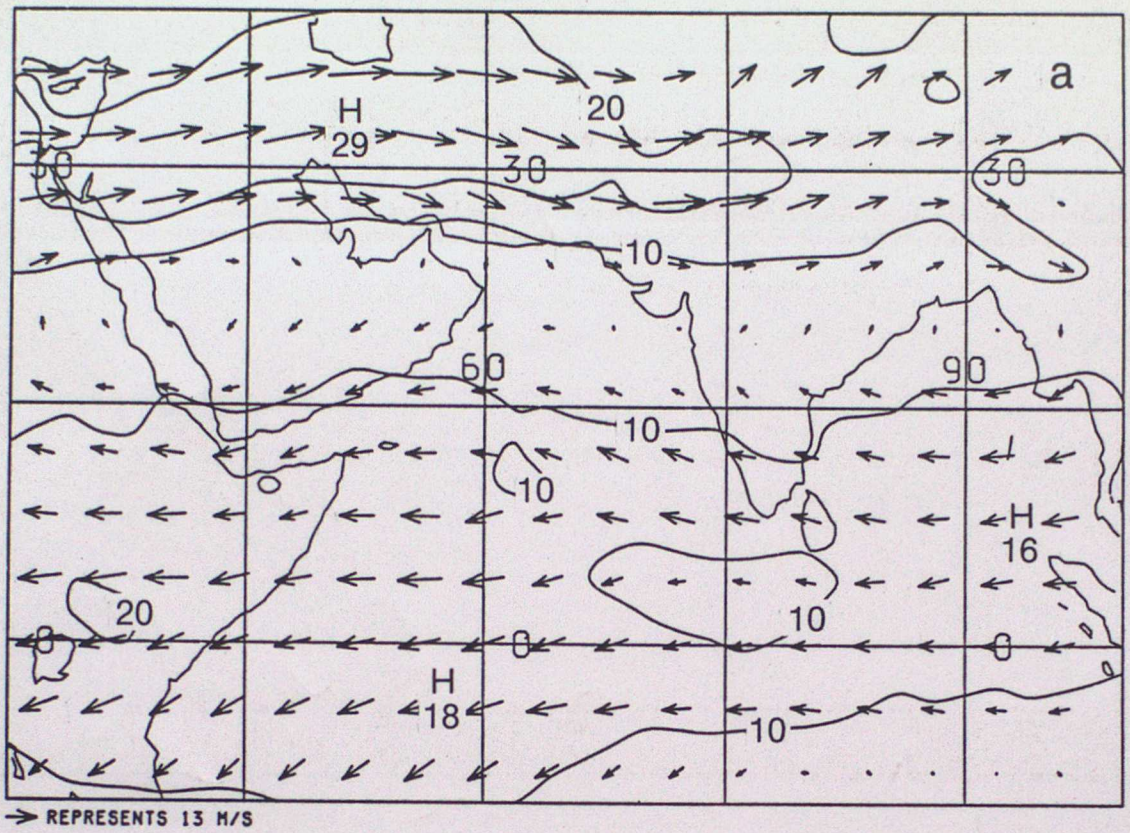
a
H
29
20
30
30
30
10
60
90
10
10
H
16
20
10
0
0
0
H
18
10
→ REPRESENTS 13 M/S

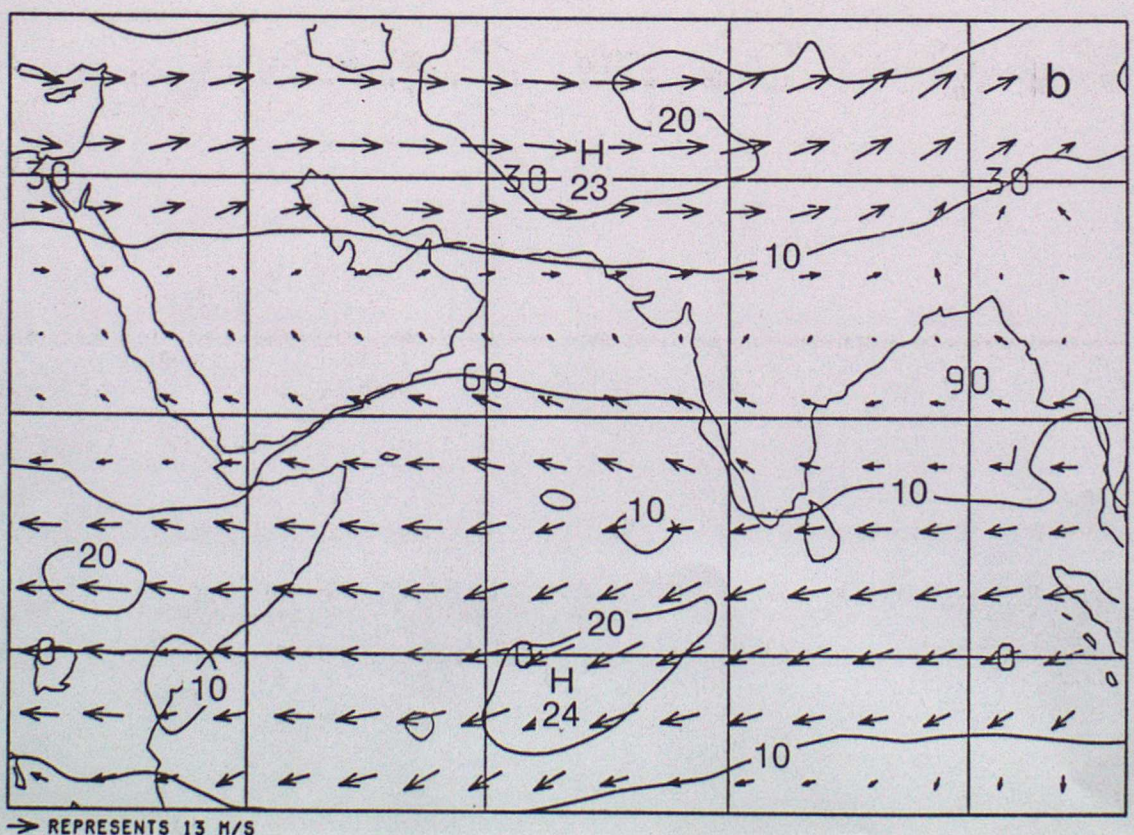
b
20
H
30
30
23
30
10
60
90
10
10
20
20
0
0
0
10
H
24
10
→ REPRESENTS 13 M/S

fig. 7a, b

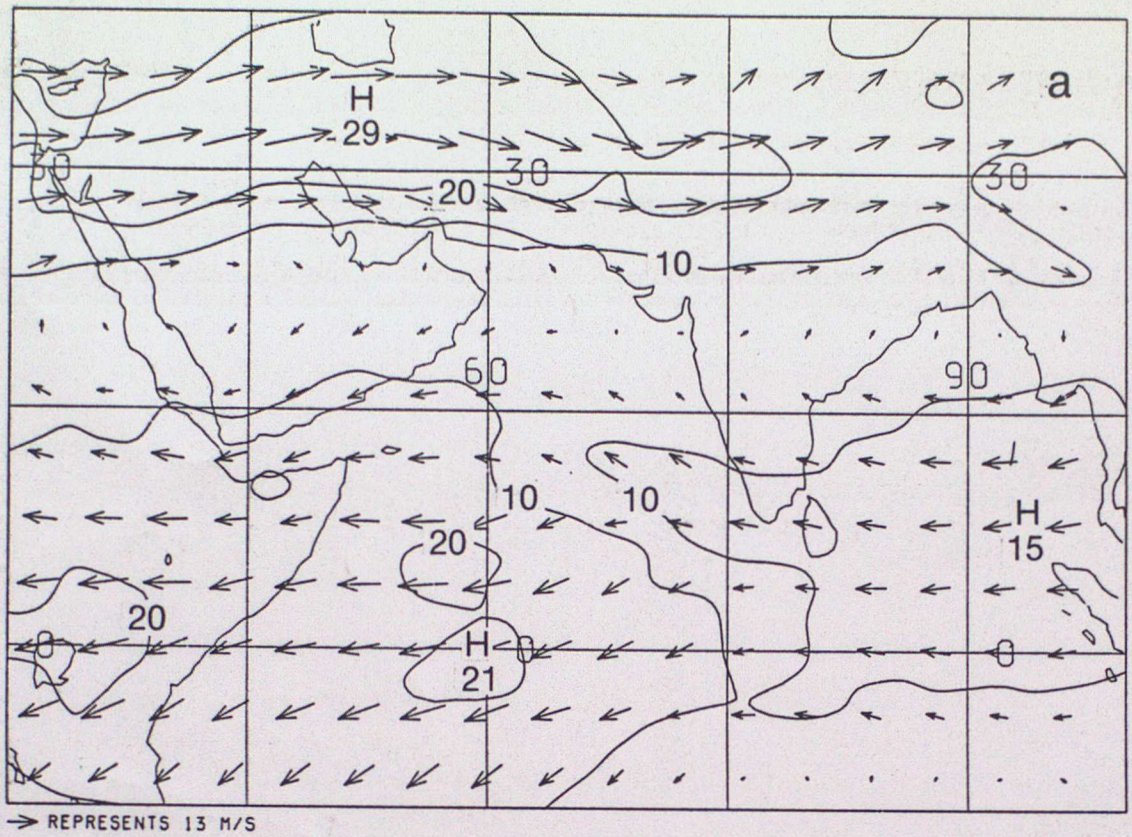
a
H
29
30
20
30
30
10
60
90
10
10
H
15
20
20
H
21
0
0
0
→ REPRESENTS 13 M/S

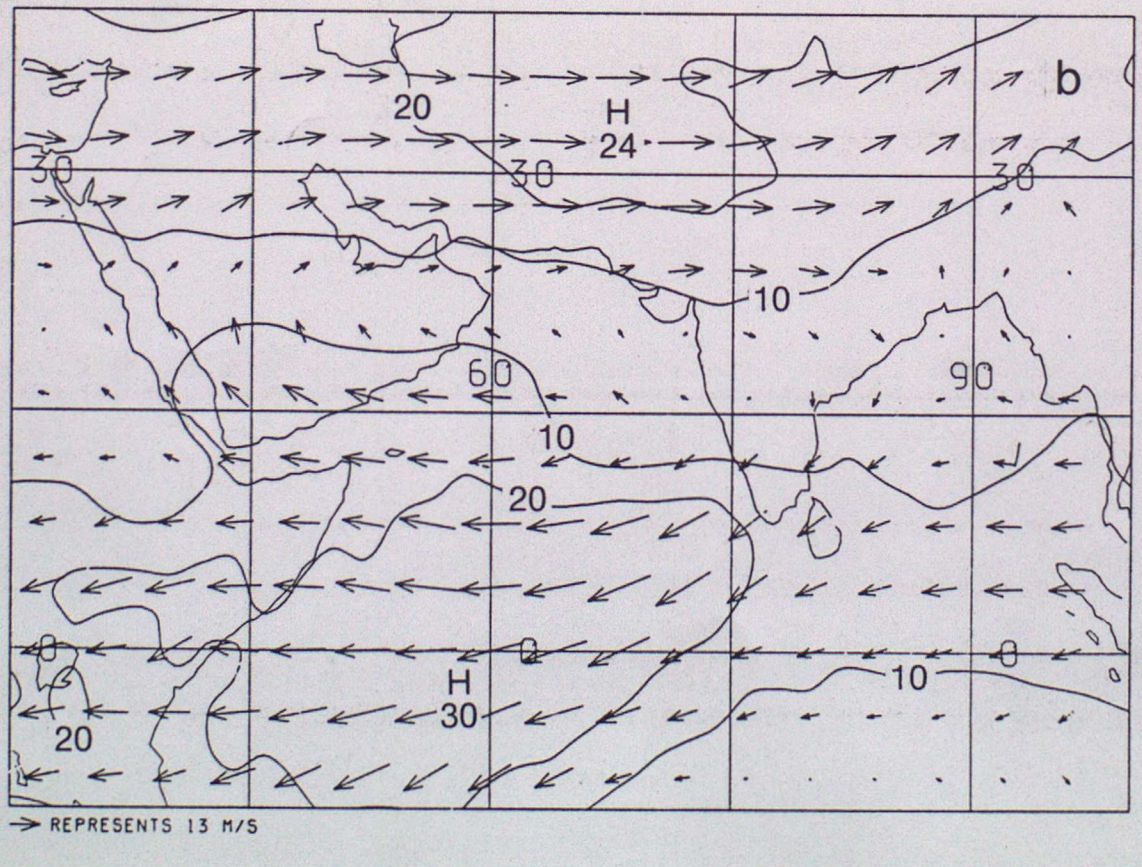
b
20
H
24
30
30
30
10
60
90
10
20
0
0
H
30
10
20
→ REPRESENTS 13 M/S

fig. 8 a,b

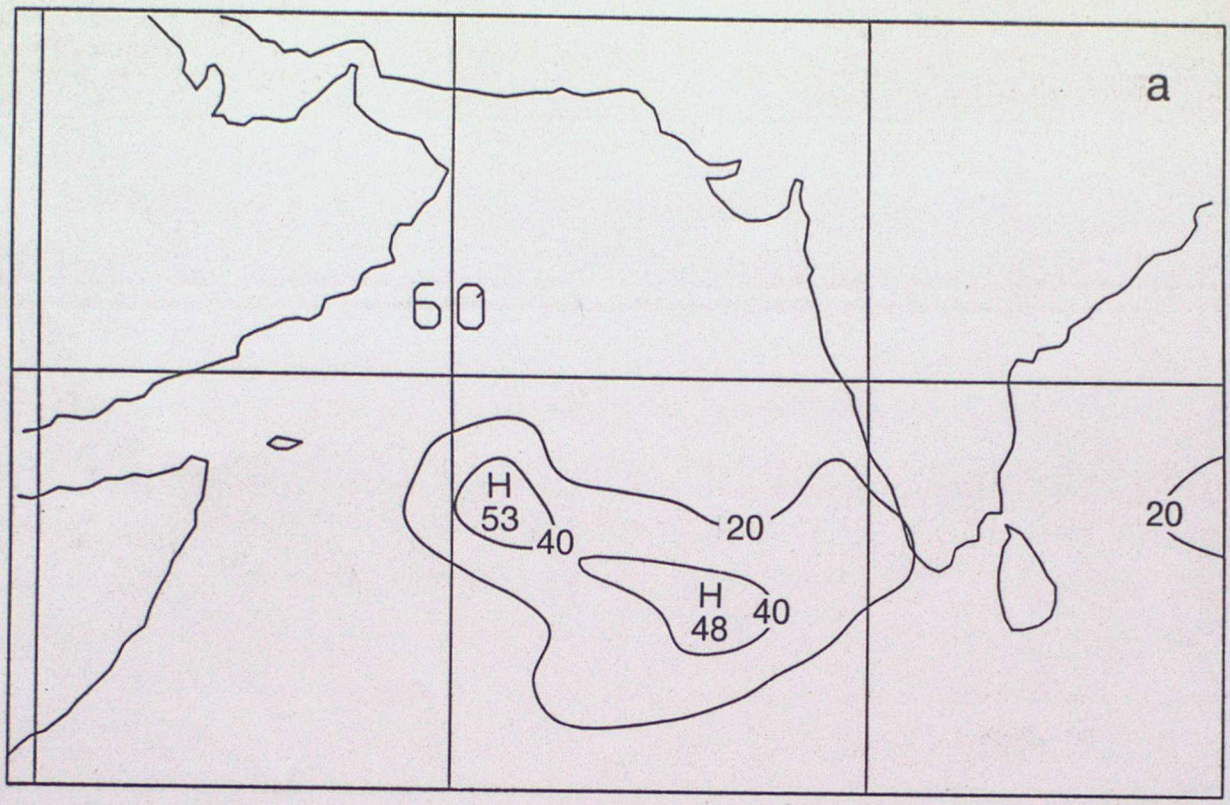

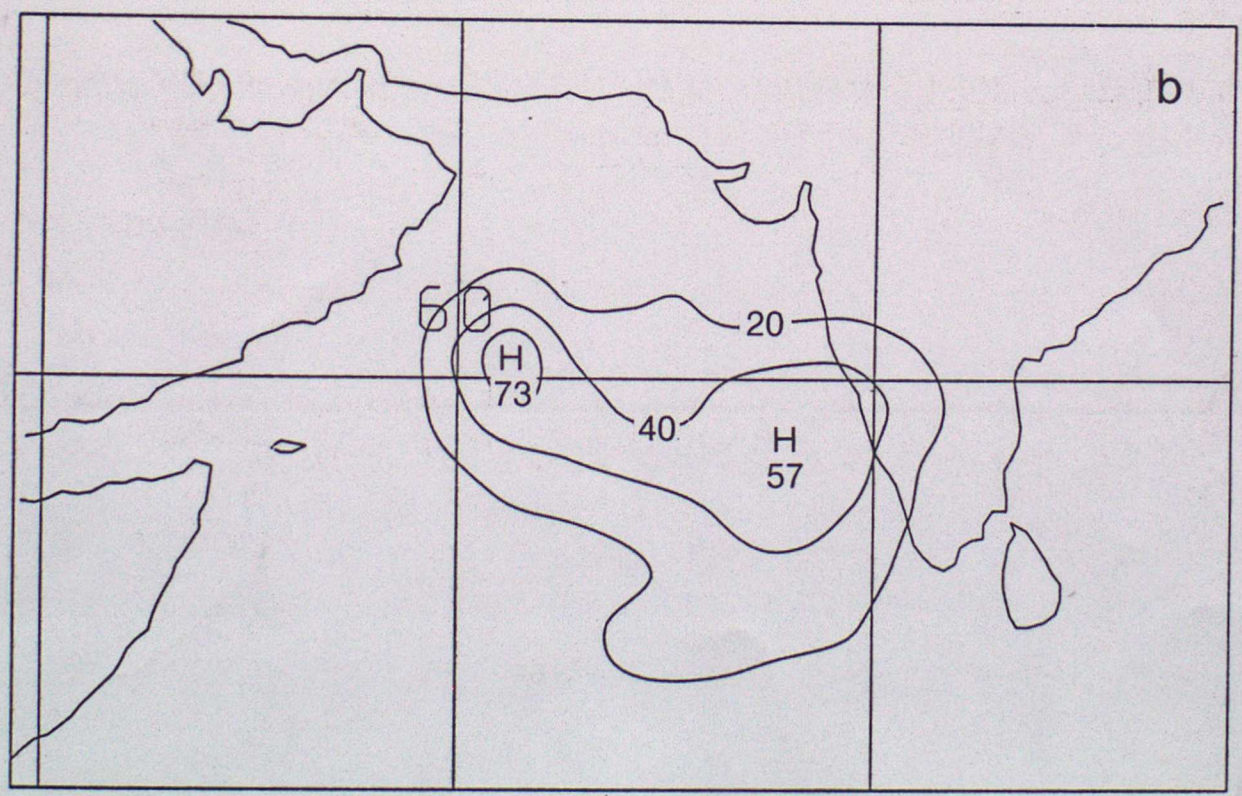

fig. 9 a,b

fig. 10

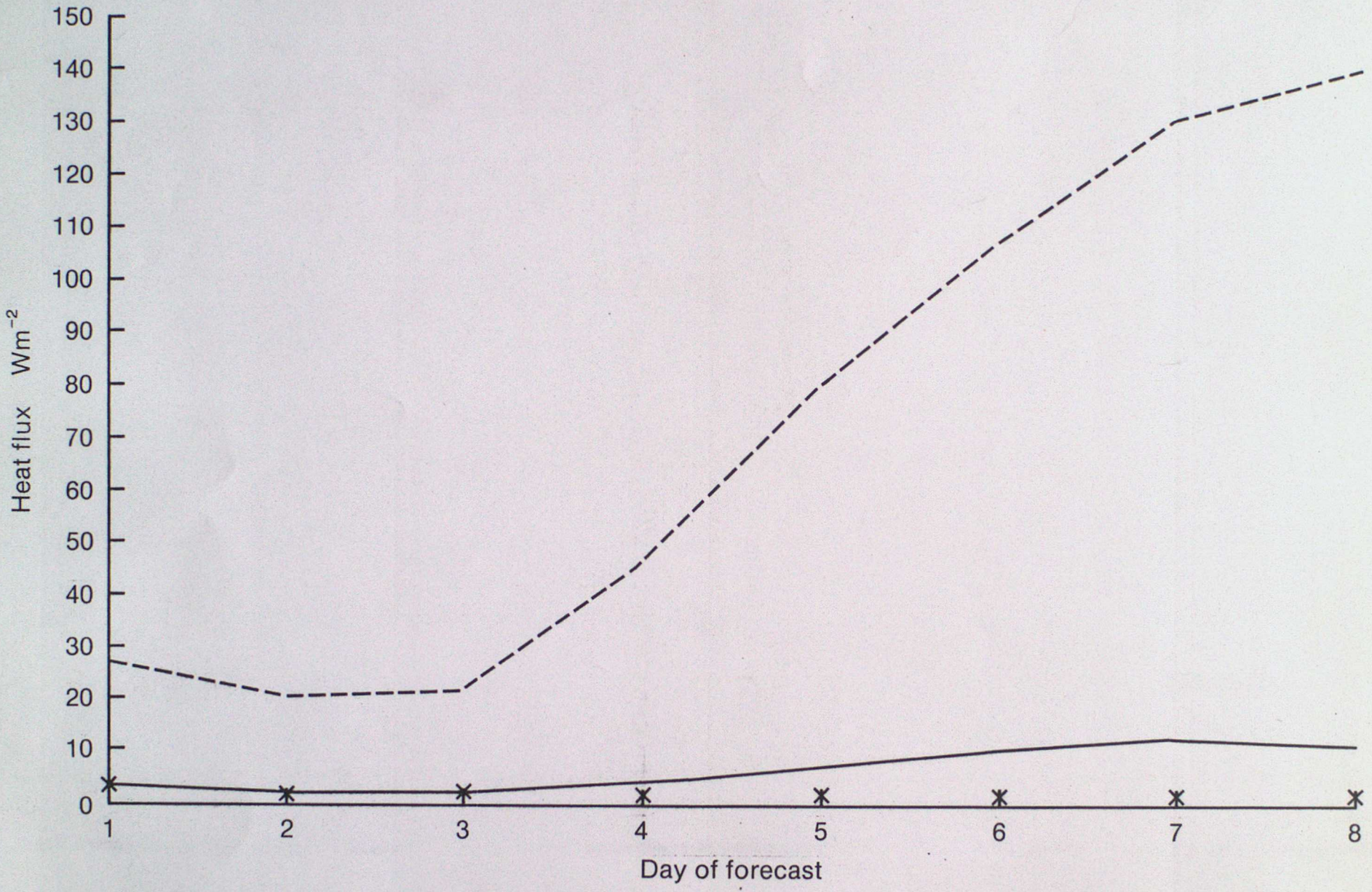
150
140
130
120
110
100
90
80
70
60
50
40
30
20
10
0
Heat flux Wm^{-2}
1
2
3
4
5
6
7
8
Day of forecast

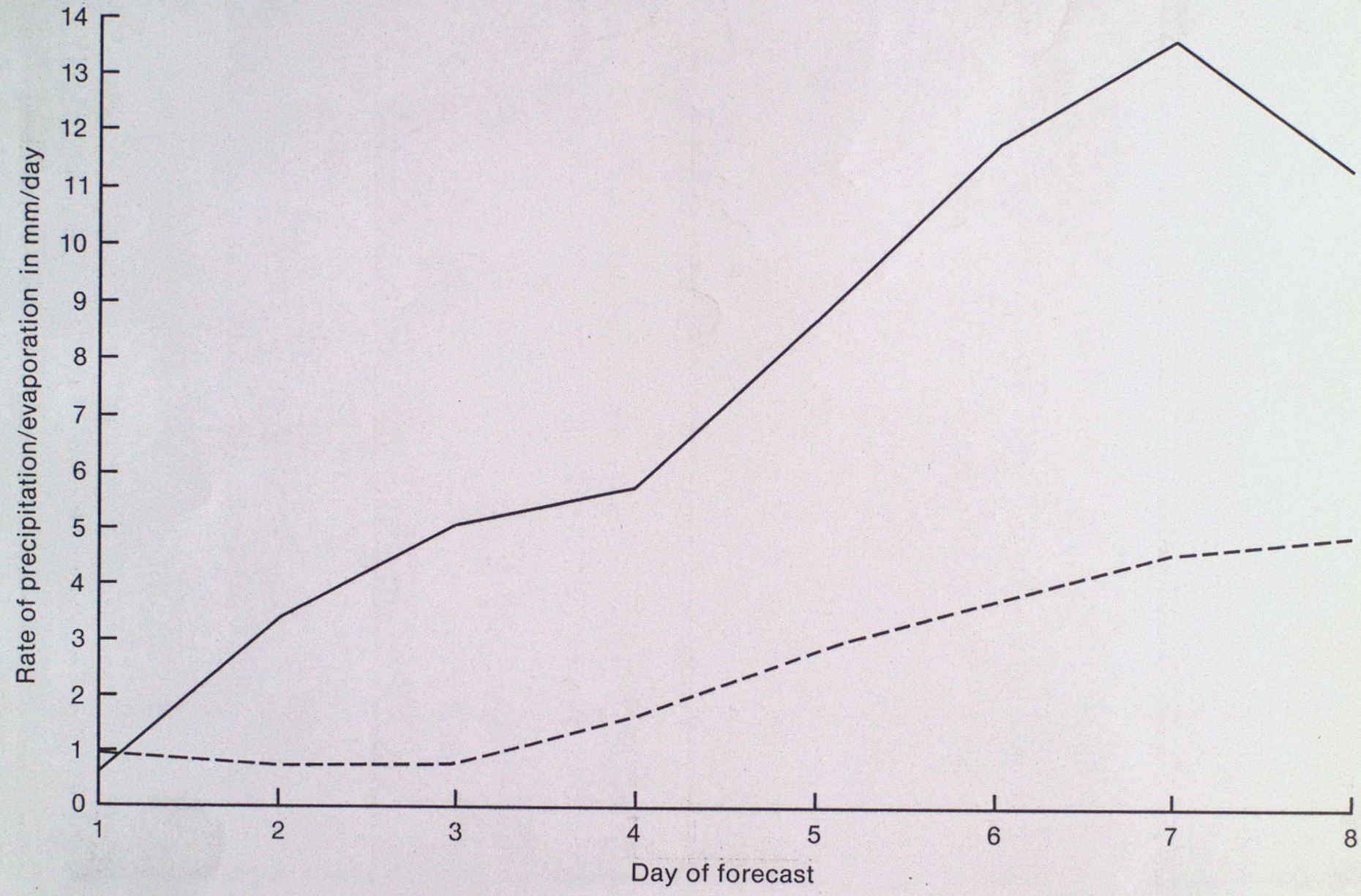
Rate of precipitation/evaporation in mm/day
0
1
2
3
4
5
6
7
8
9
10
11
12
13
14
1
2
3
4
5
6
7
8
Day of forecast

fig. 11

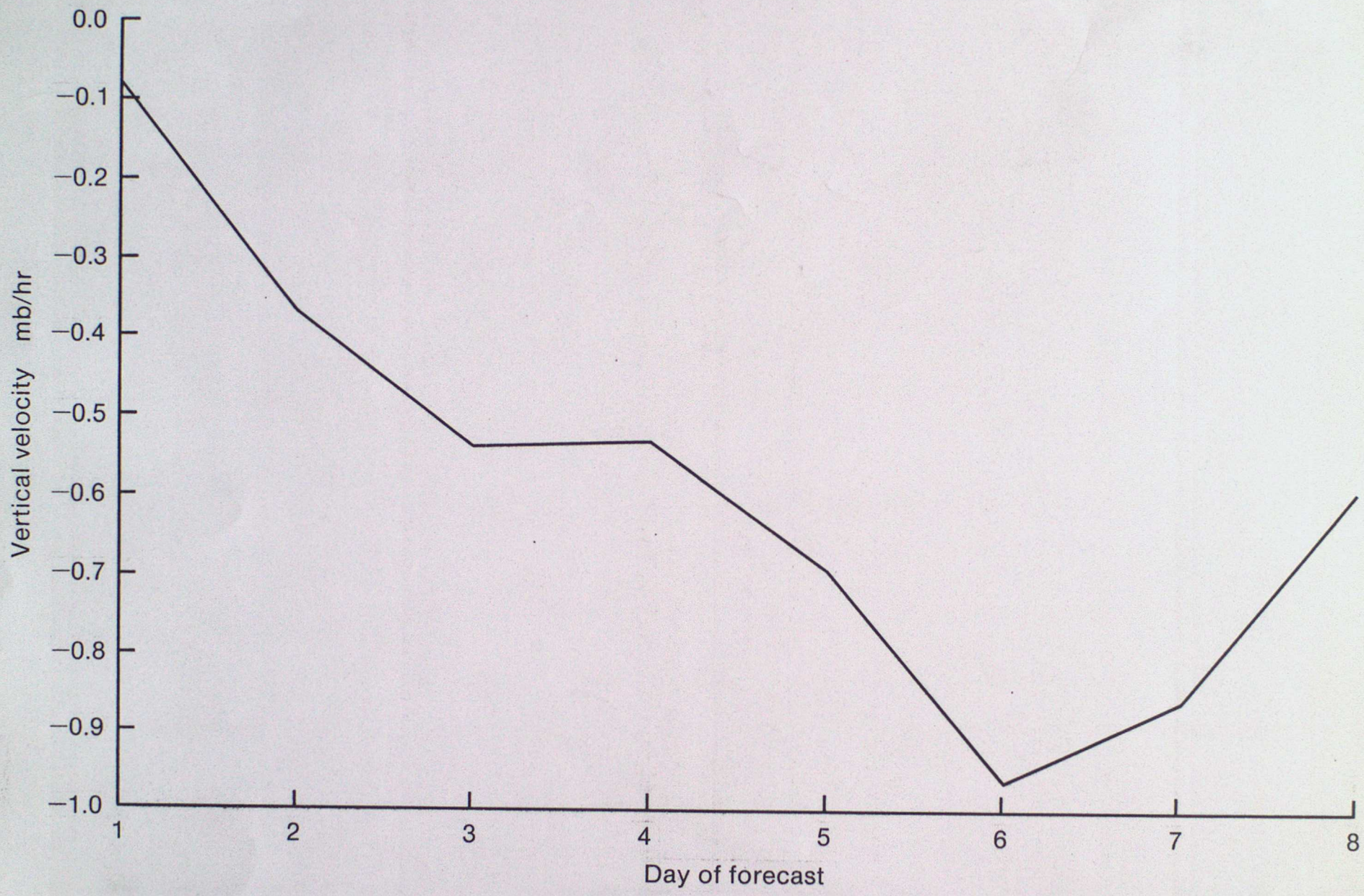
0.0
−0.1
−0.2
−0.3
−0.4
−0.5
−0.6
−0.7
−0.8
−0.9
−1.0
Vertical velocity mb/hr
1
2
3
4
5
6
7
8
Day of forecast

fig. 12

fig. 13

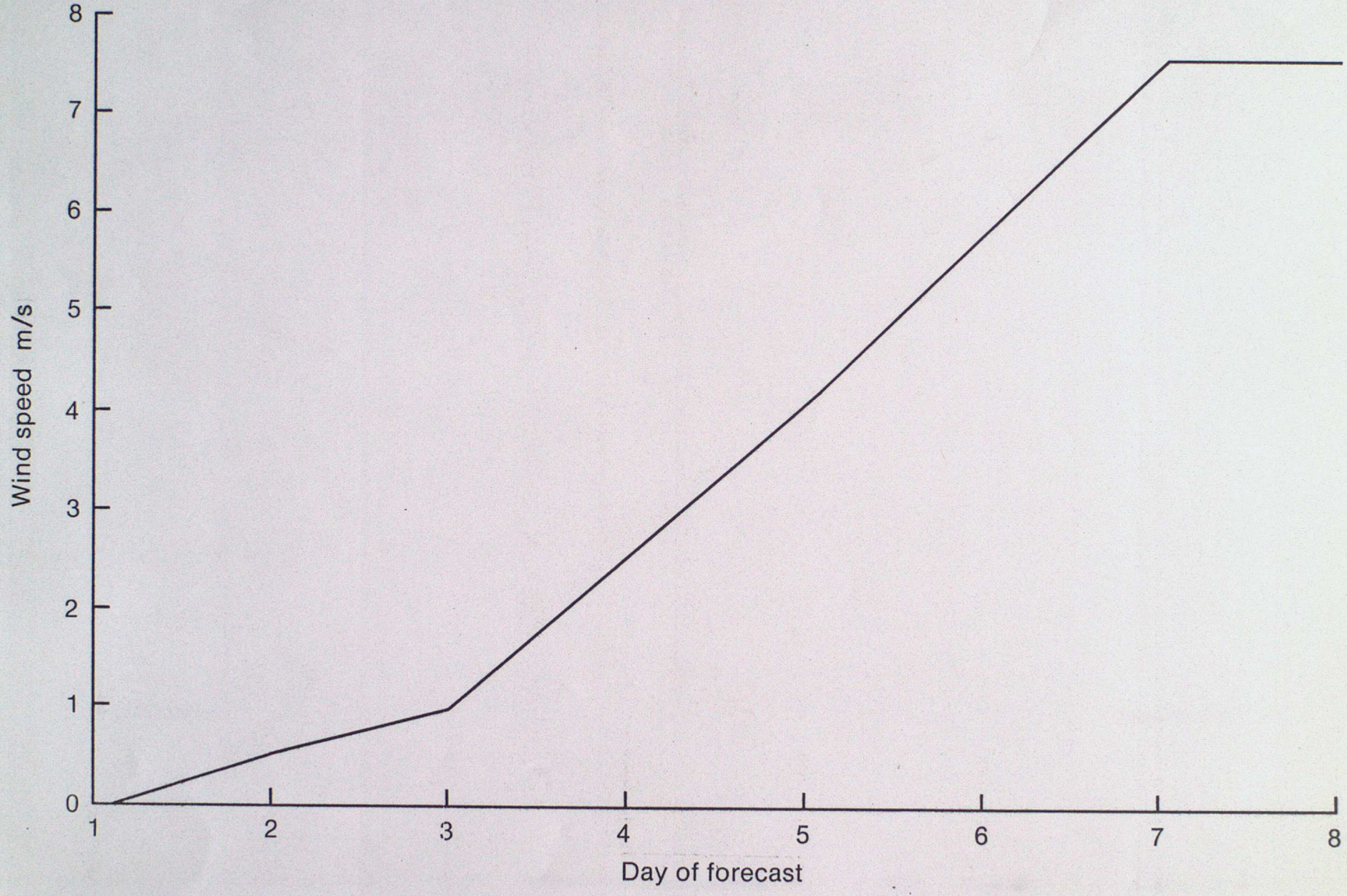

fig. 14

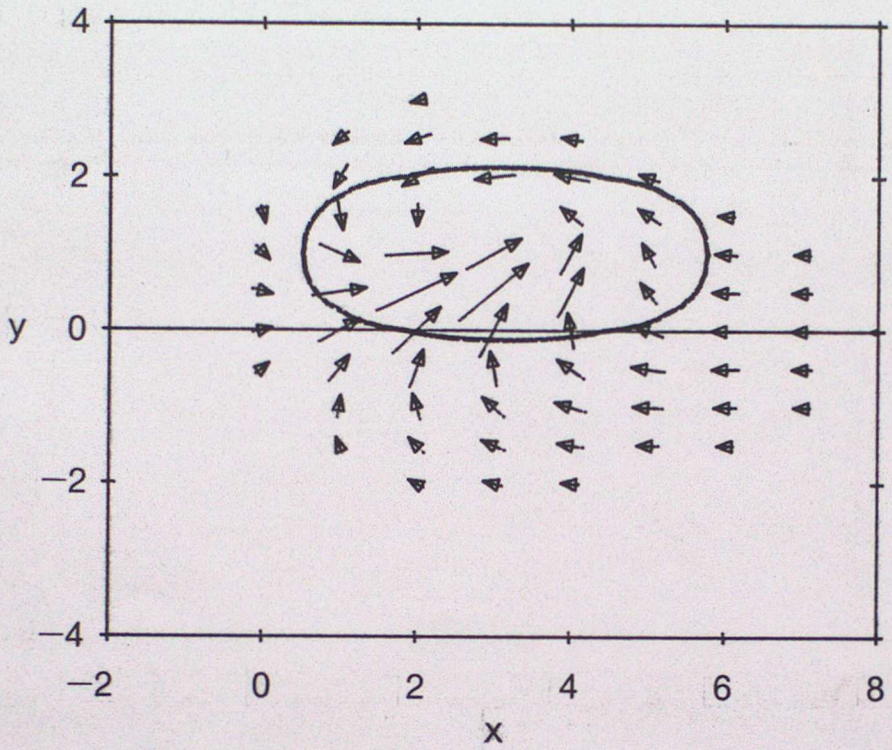

fig. 15

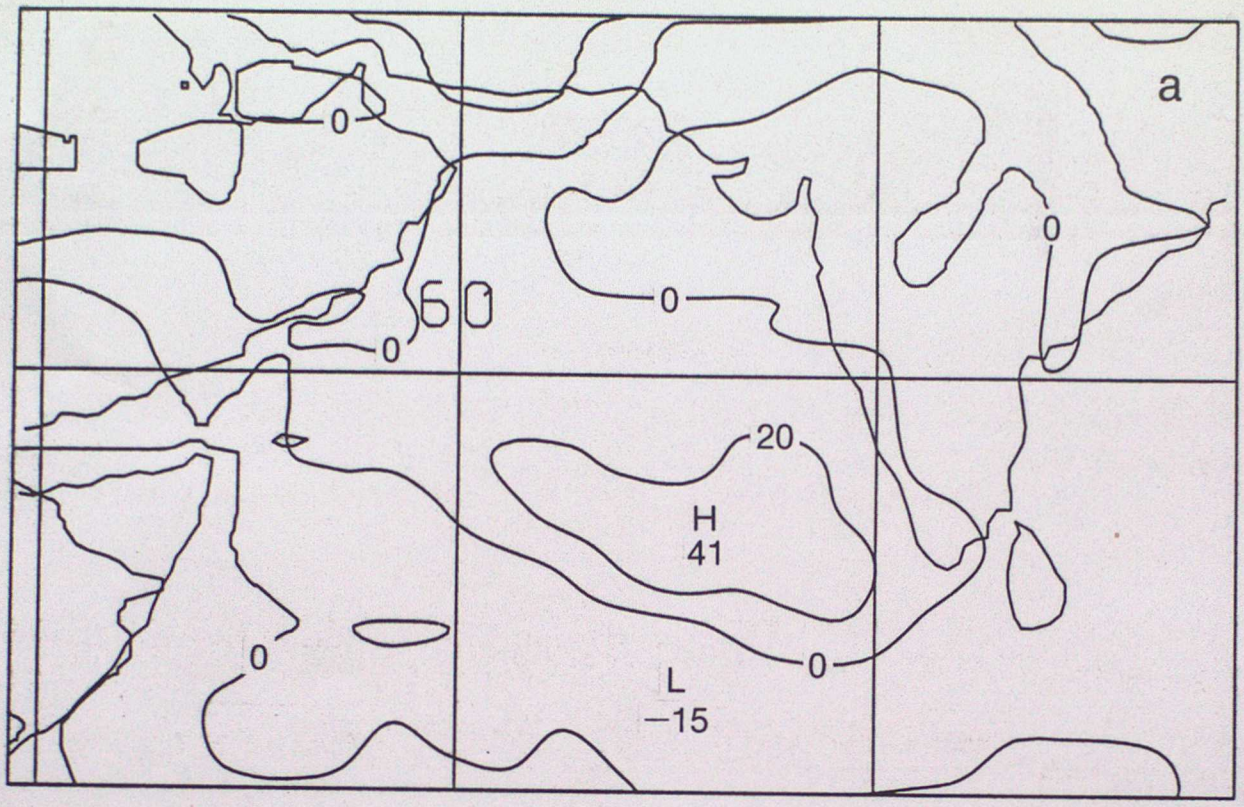

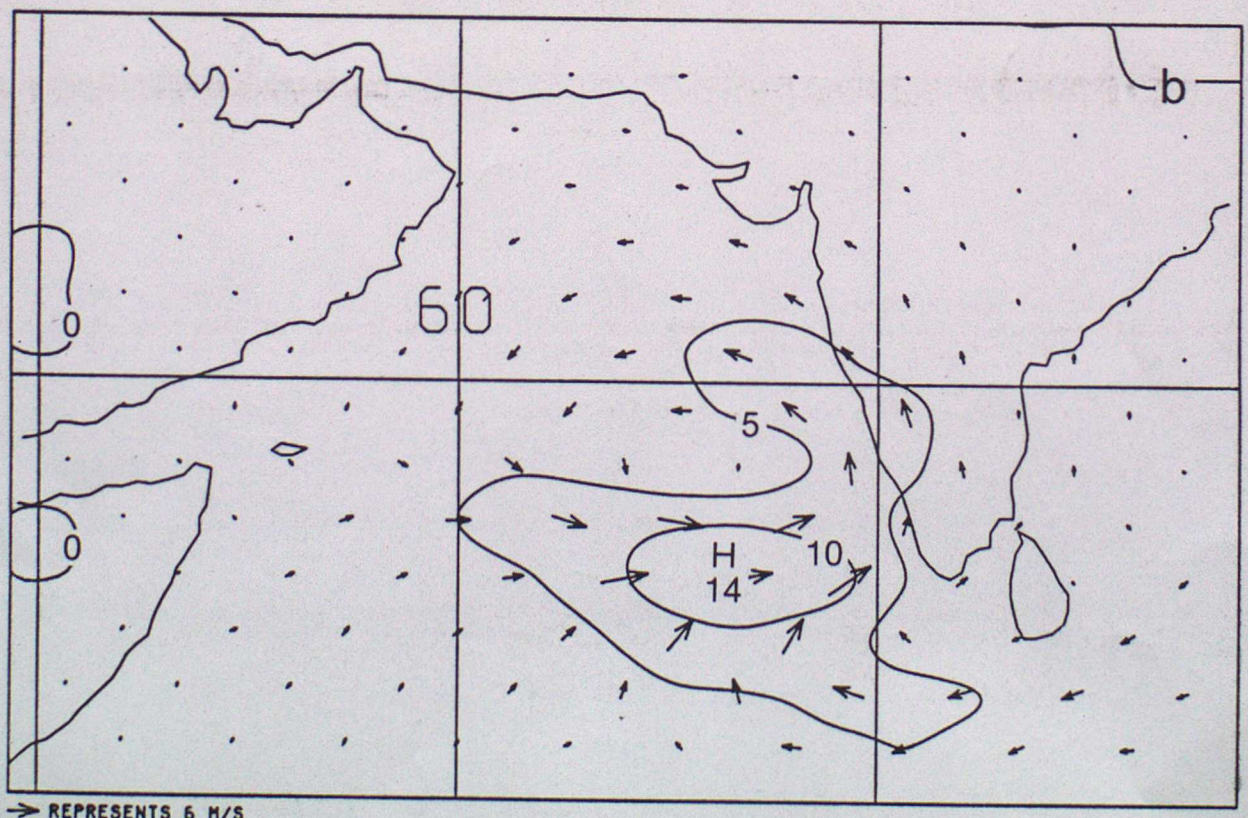

fig. 16 a, b

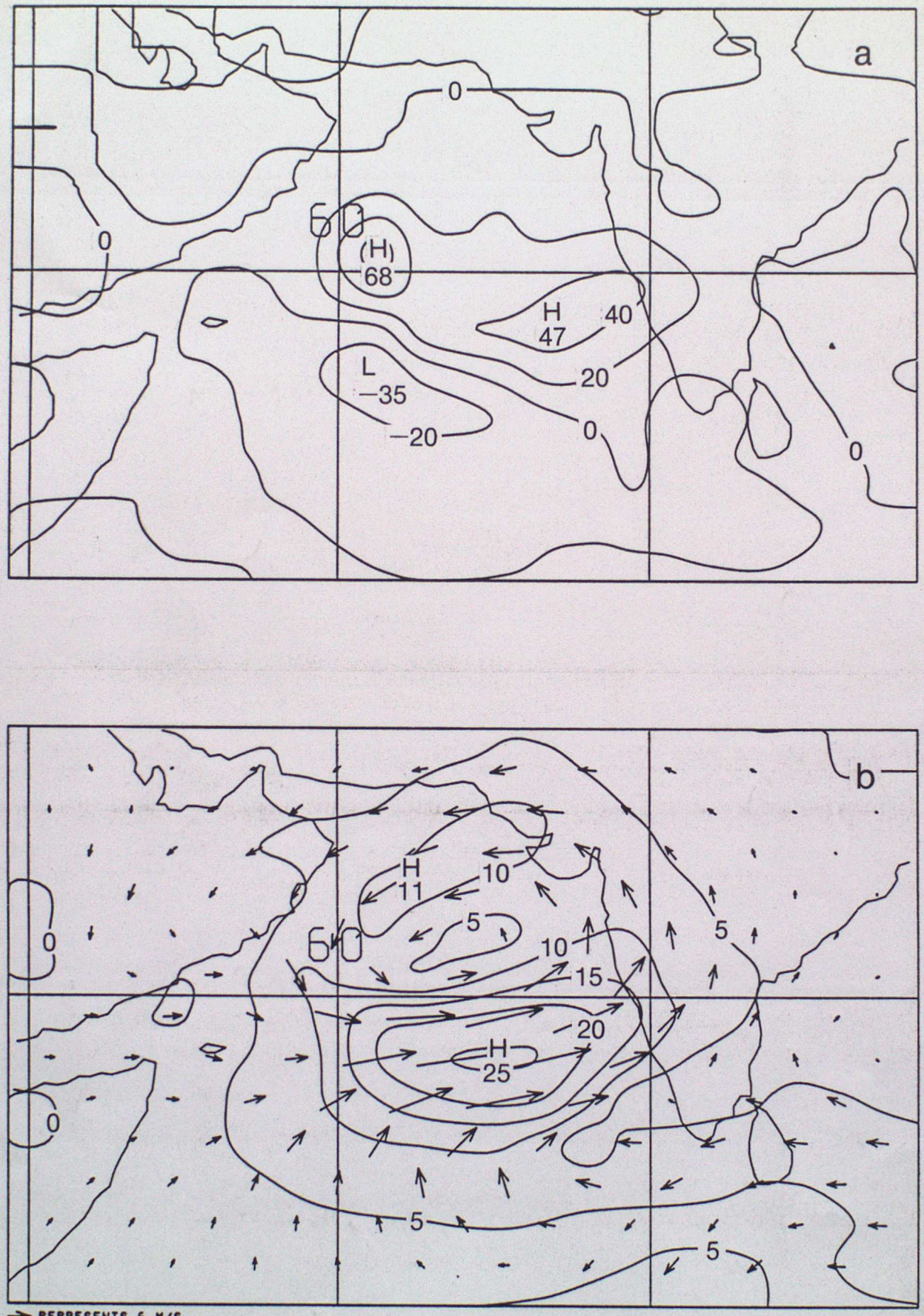
a
0
60
(H)
68
H
47
40
20
L
−35
−20
0
0
0
b
H
11
10
5
60
10
15
20
H
25
0
0
5
5
5
→ REPRESENTS 6 M/S

fig. 17 a, b

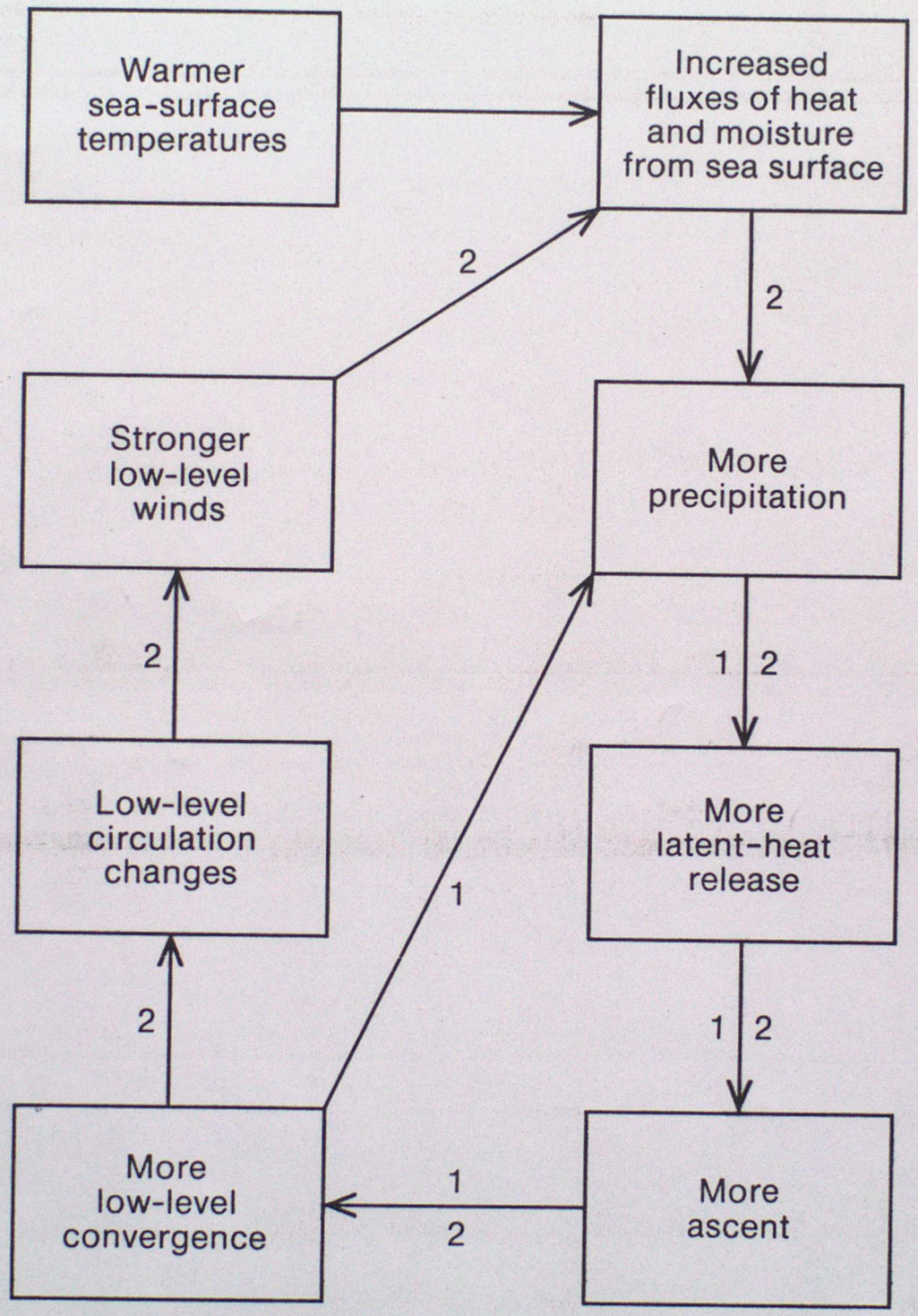
Warmer sea-surface temperatures
Increased fluxes of heat and moisture from sea surface
2
2
Stronger low-level winds
More precipitation
2
1 2
Low-level circulation changes
More latent-heat release
1
2
1 2
More low-level convergence
1
2
More ascent

fig. 18

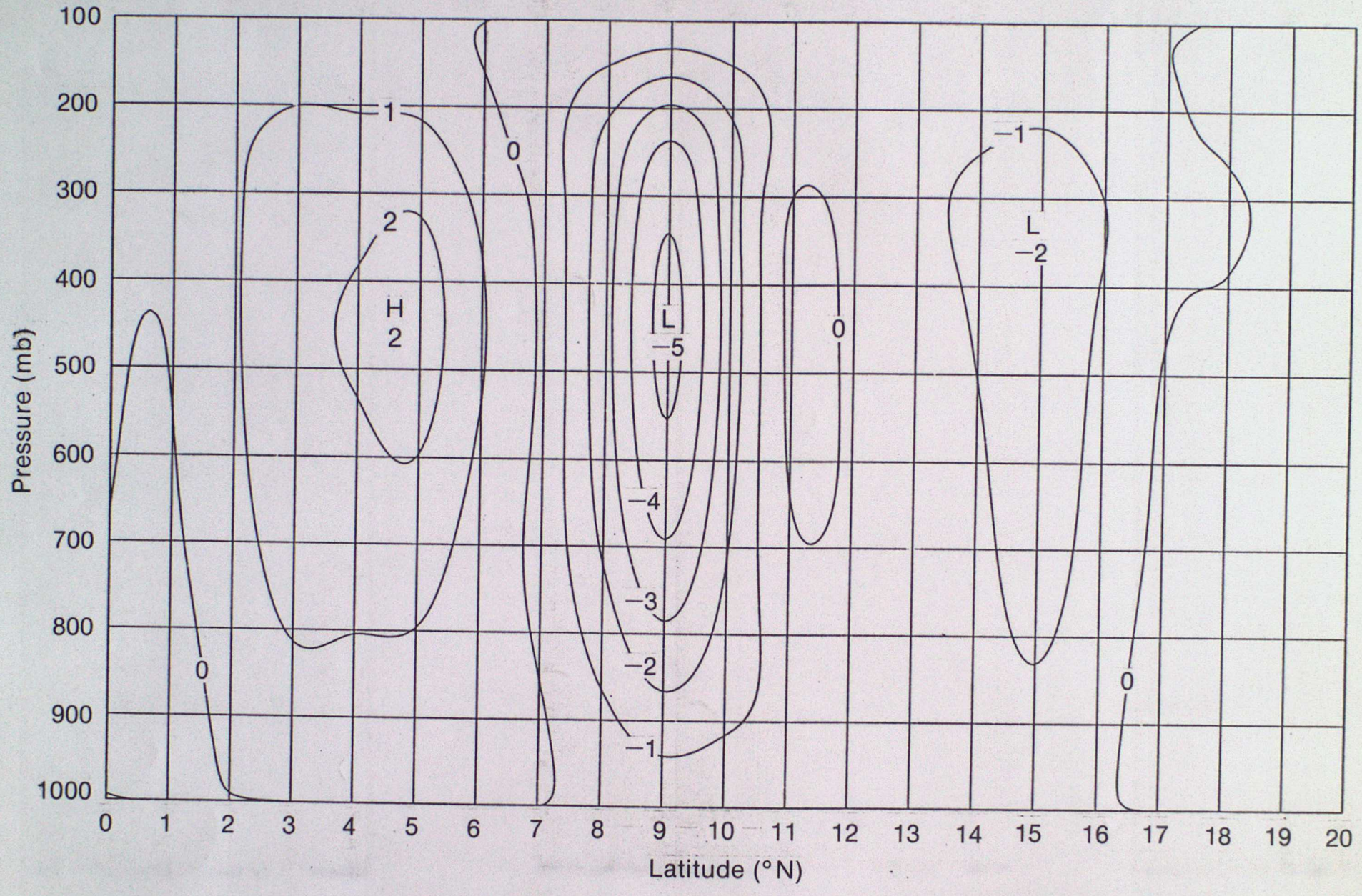
Pressure (mb)
100
200
300
400
500
600
700
800
900
1000
0 1 2 3 4 5 6 7 8 9 10 11 12 13 14 15 16 17 18 19 20
Latitude (°N)
1
2
H
2
0
0
L
−5
−4
−3
−2
−1
0
−1
L
−2
0

fig. 19

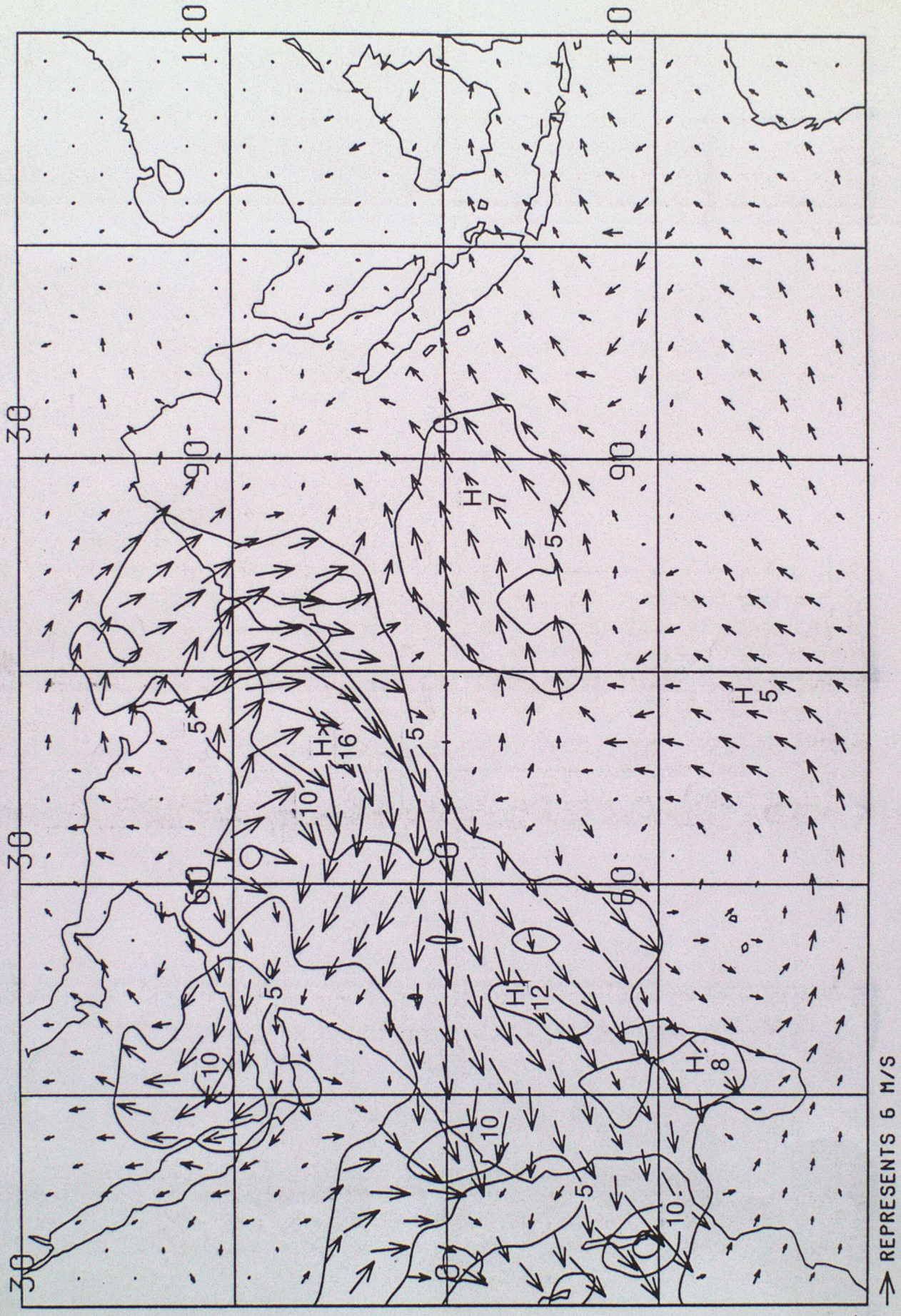

120
120
30
90
90
30
60
60
30
0
0
0
H 7
H 5
H 16
H 12
H 8
5
10
REPRESENTS 6 M/S

fig. 20

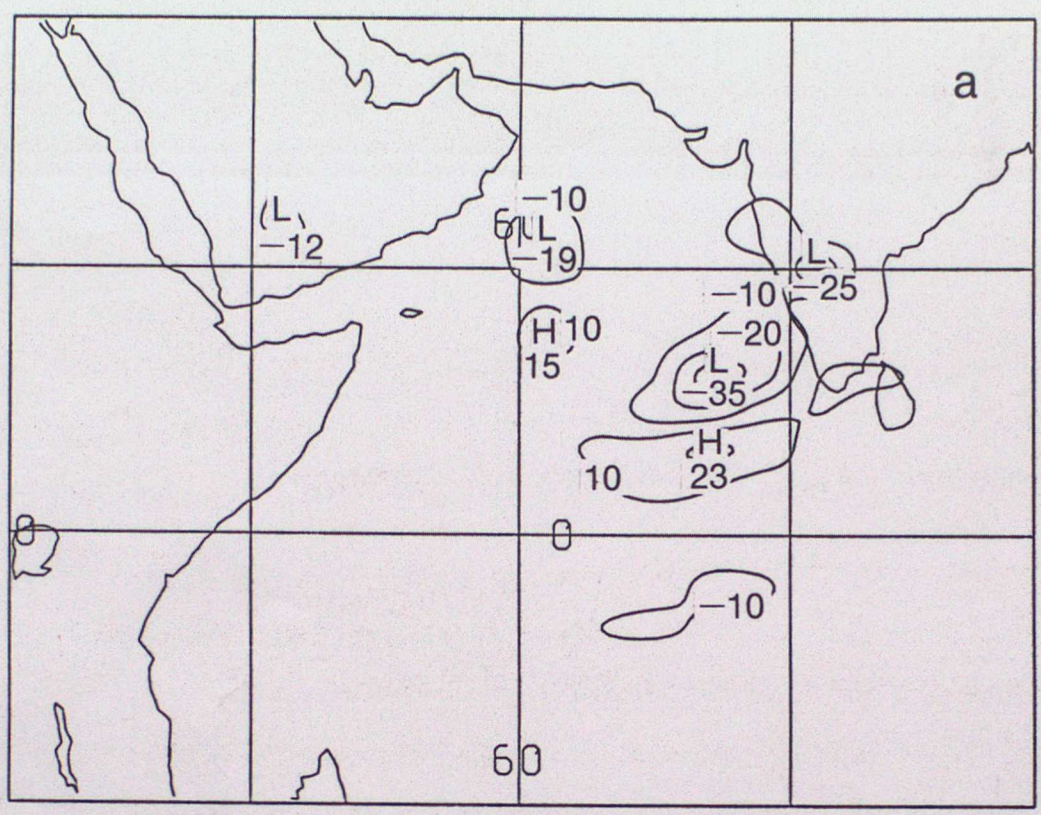
a
(L)
−12
−10
(L)
−19
(L)
−25
−10
H 10
15
−20
(L)
−35
(H)
10
23
0
0
−10
60

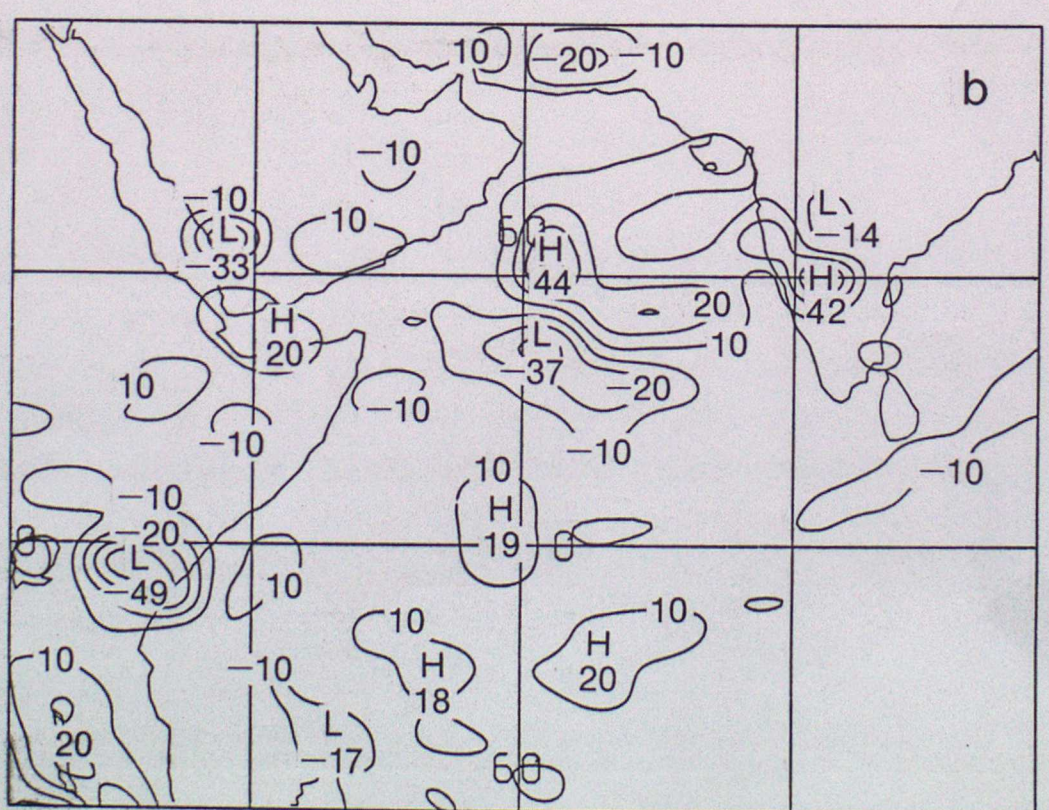
b
10
−20
−10
−10
−10
(L)
−33
10
(L)
−14
H
44
(H)
42
20
H
20
10
(L)
−37
−20
10
−10
−10
−10
10
H
19
−10
−10
−20
(L)
−49
10
10
10
H
20
10
−10
H
18
20
(L)
−17
60

fig. 21 a,b

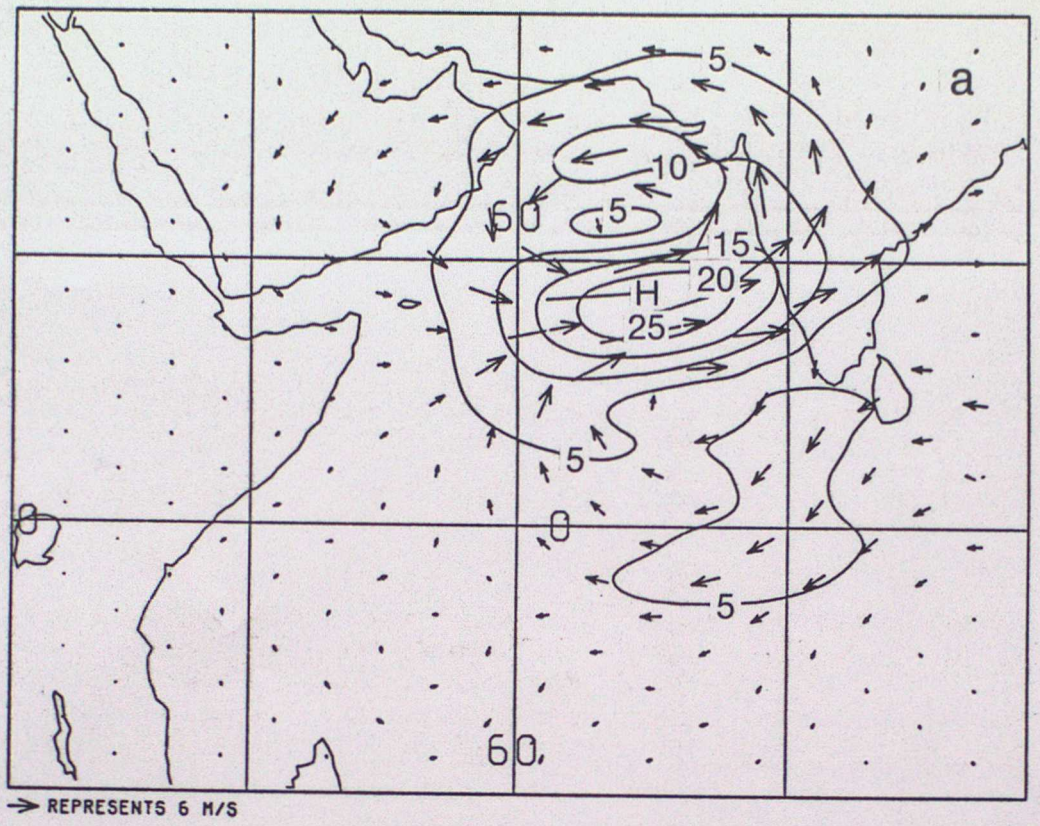
a
5
10
5
15
H
20
25
5
0
0
5
60
REPRESENTS 6 M/S

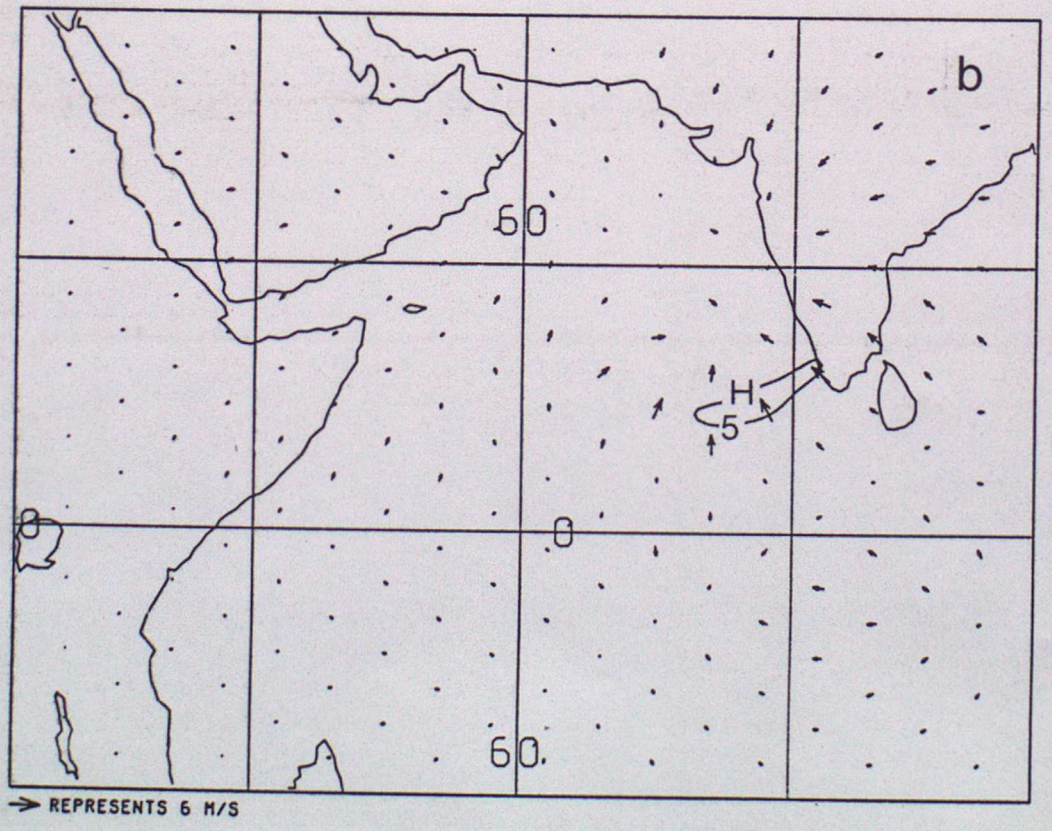
b
60
H
5
0
0
60
REPRESENTS 6 M/S

fig. 22 a,b

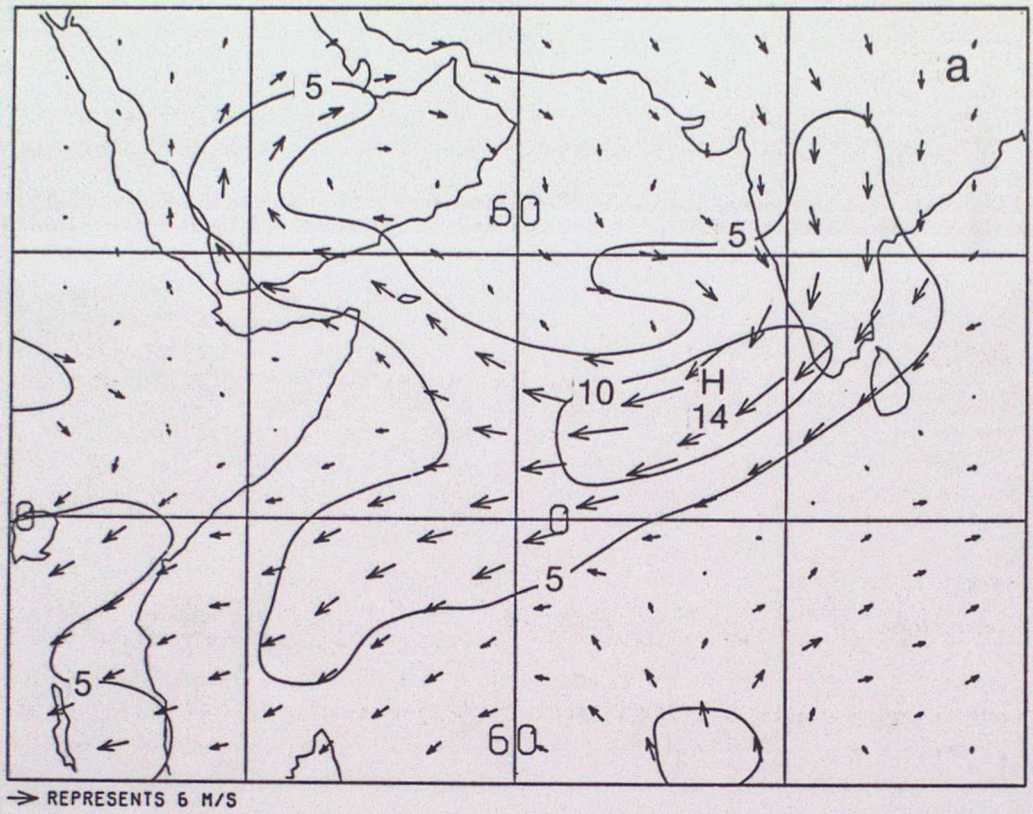
a
5
60
5
H
10
14
0
0
5
5
60
→ REPRESENTS 6 M/S

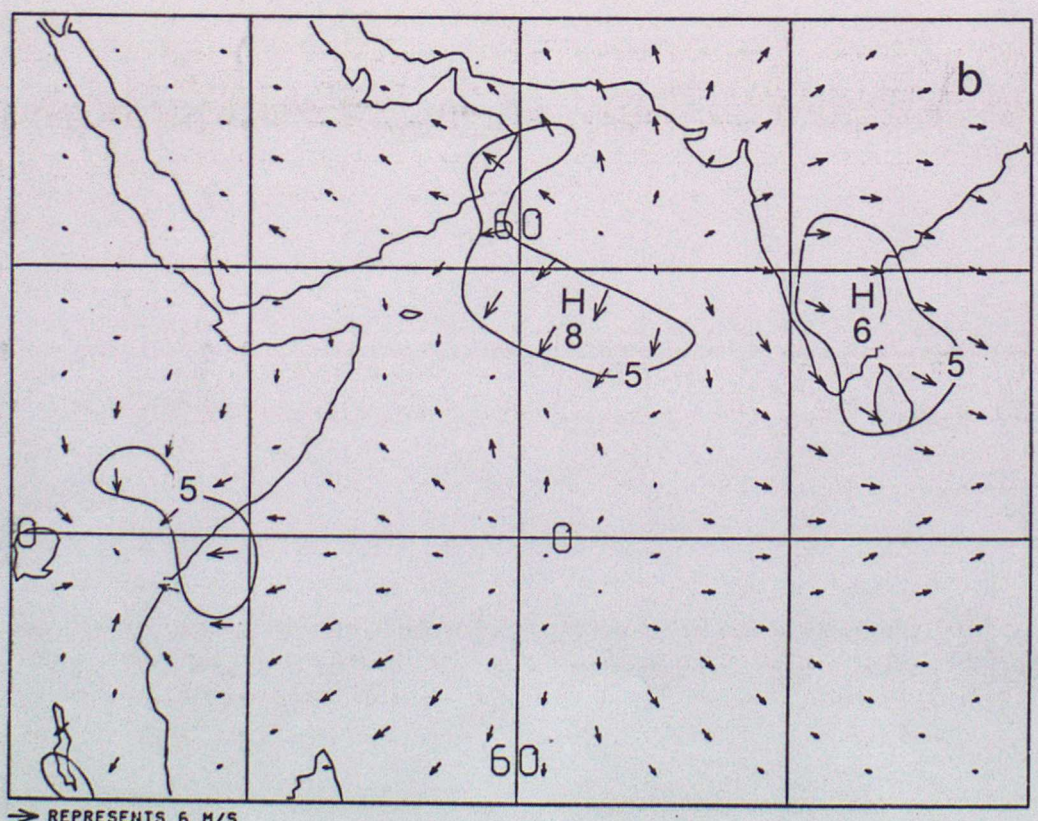
b
60
H
8
5
H
6
5
5
0
0
60
→ REPRESENTS 6 M/S

fig. 23 a, b

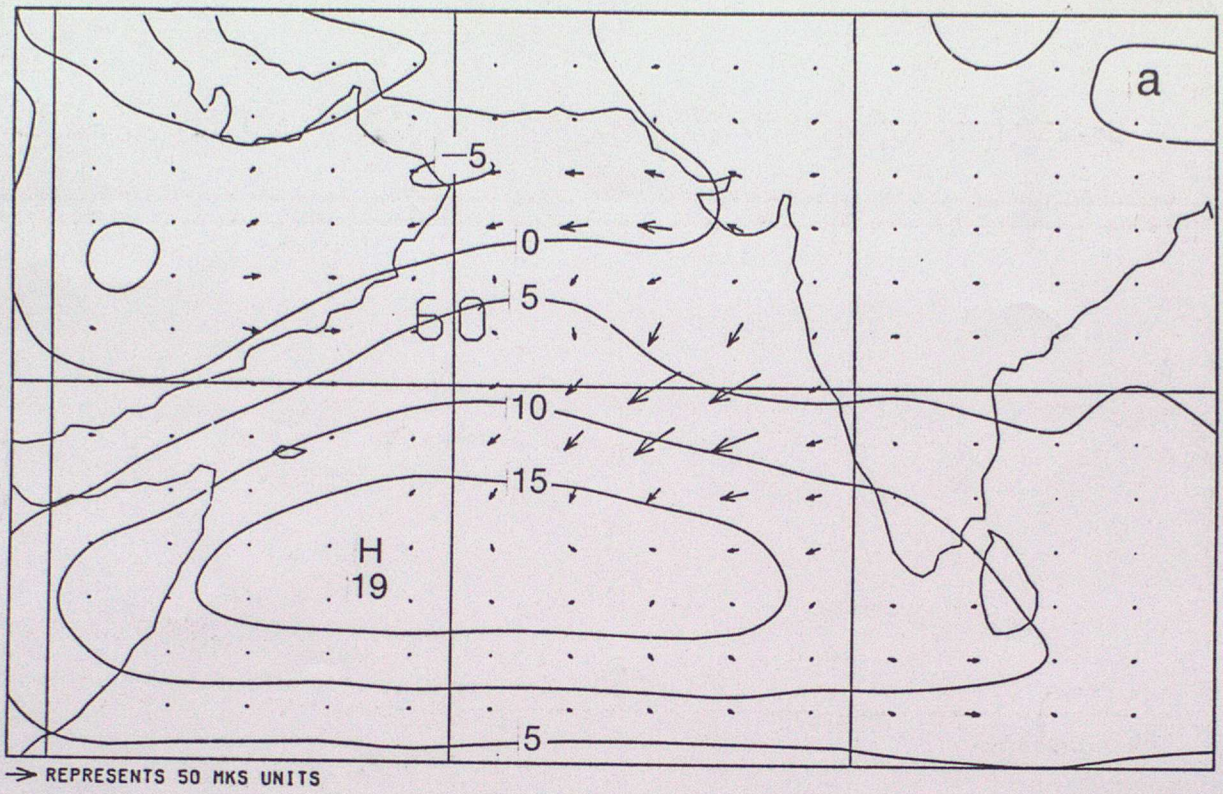
a
−5
0
5
60
10
15
H
19
5
→ REPRESENTS 50 MKS UNITS

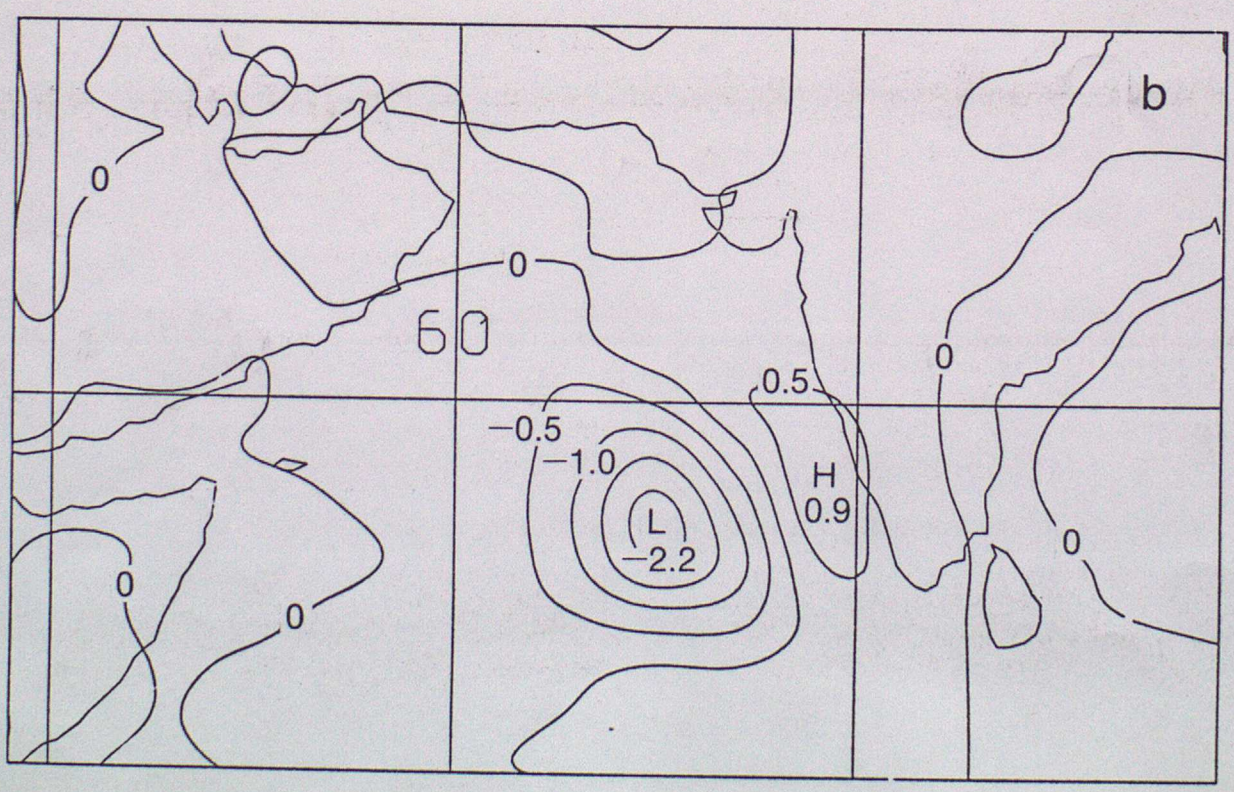
b
0
0
60
0.5
0
−0.5
−1.0
H
0.9
L
−2.2
0
0
0

fig. 24 a,b

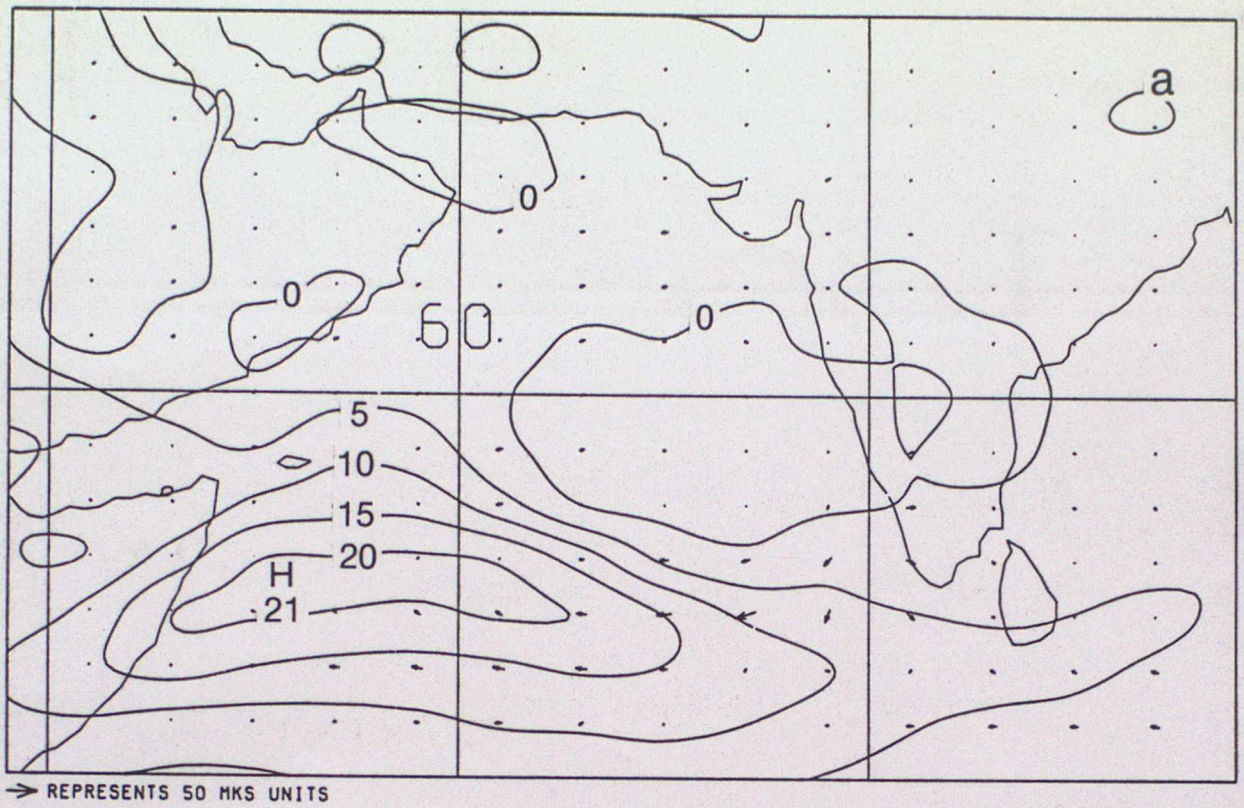
a
0
0
60
0
5
10
15
20
H
21
→ REPRESENTS 50 MKS UNITS

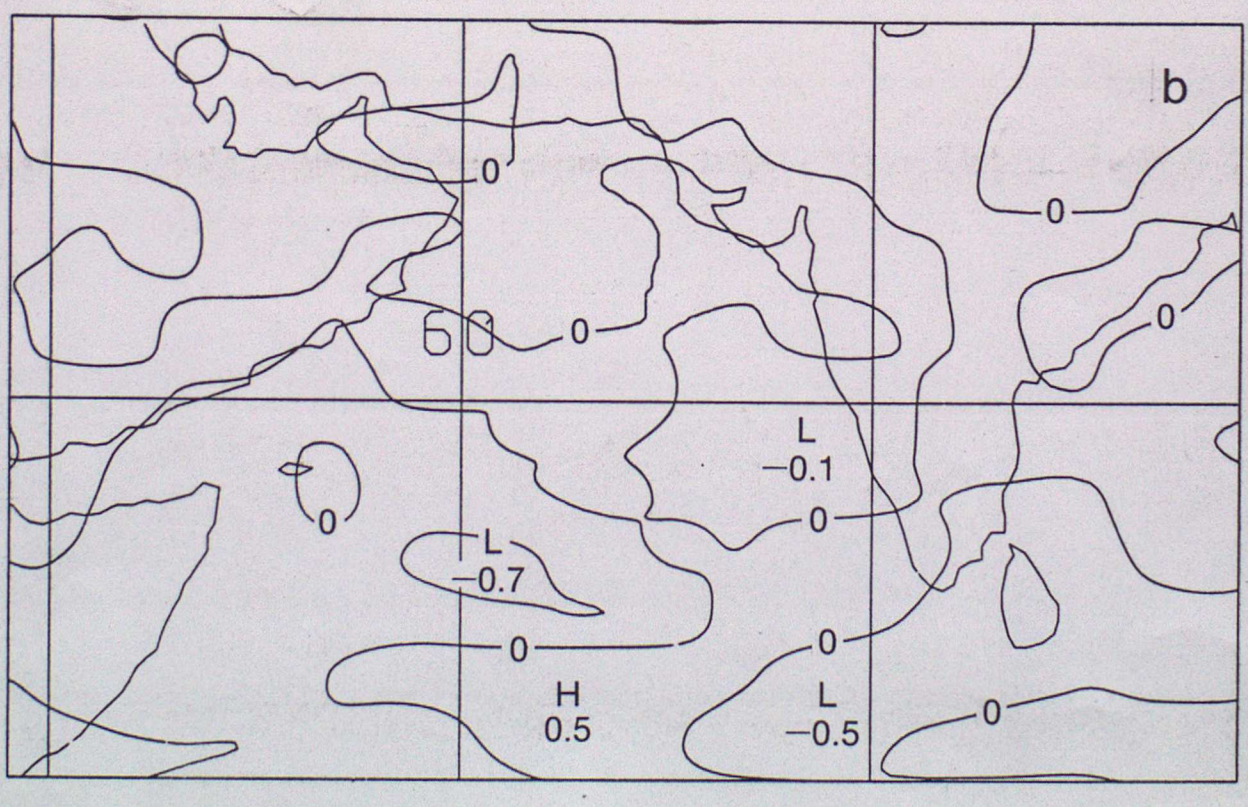
b
0
0
60
0
0
L
−0.1
0
L
−0.7
0
0
H
0.5
L
−0.5
0

fig. 25 a, b

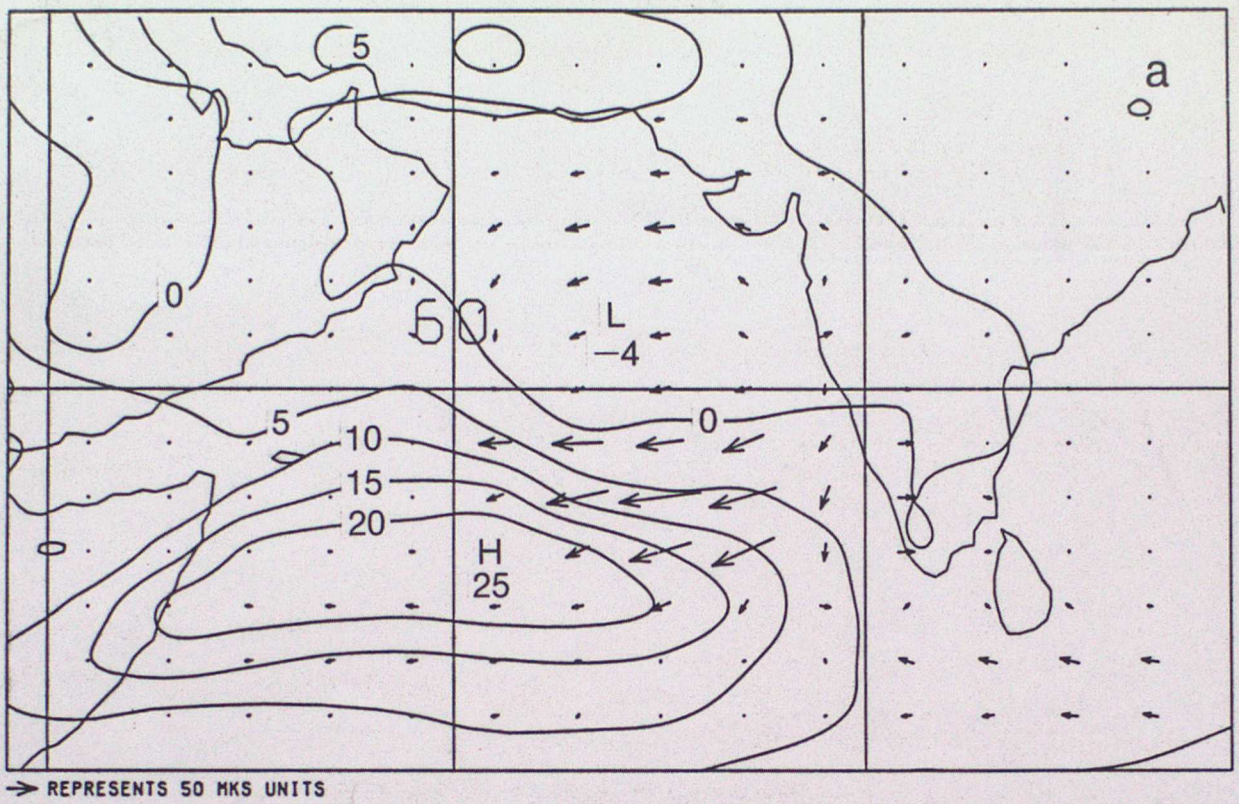
a
5
0
60
L
−4
5
10
15
20
0
H
25
→ REPRESENTS 50 MKS UNITS

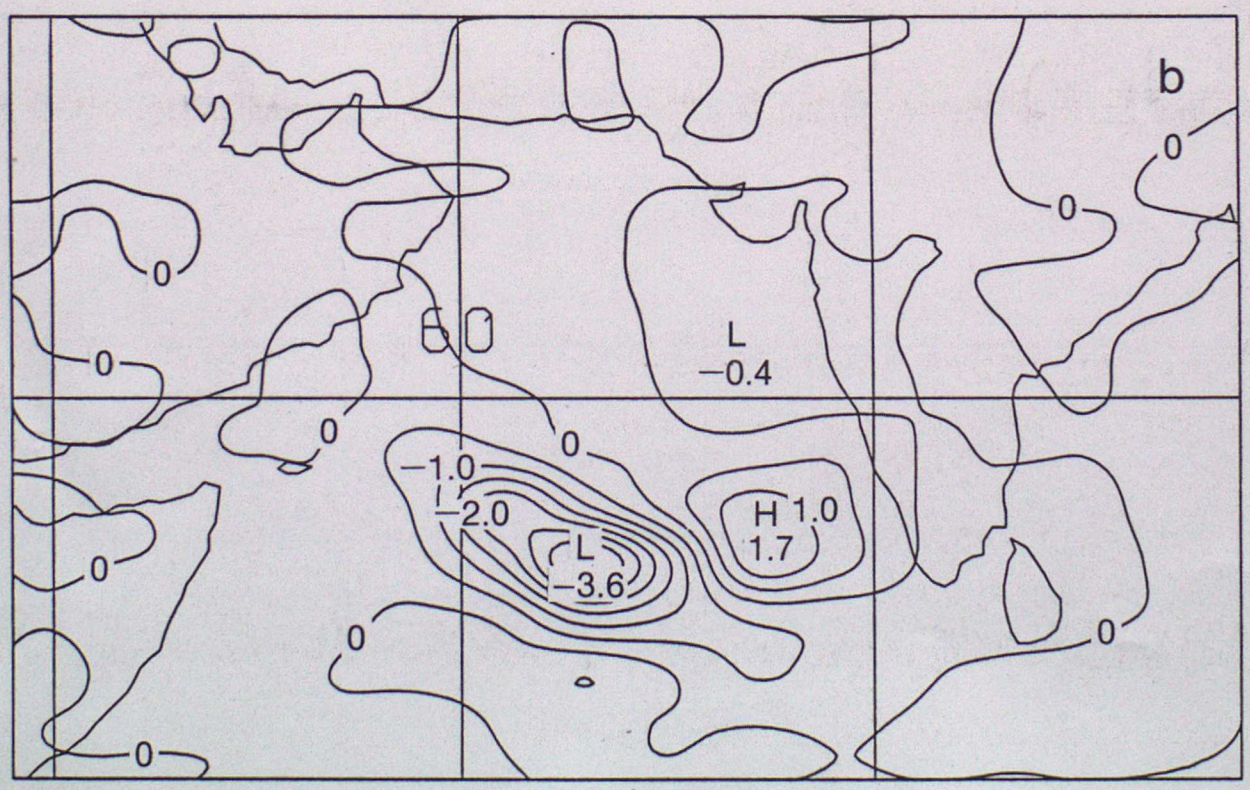
b
0
0
0
0
60
L
−0.4
0
−1.0
−2.0
L
−3.6
H 1.0
1.7
0
0
0
0

fig. 26 a,b

fig. 27

DYNAMICAL CLIMATOLOGY TECHNICAL NOTES

DCTN 1	June 1984	A scheme for incorporating the thermodynamic sea-ice model into a coupled ocean-atmosphere model. C Gordon and M Bottomley
DCTN 2	Sept 1984	The parametrization of the upper ocean mixed layer in coupled ocean/atmosphere models. C Gordon and M Bottomley
DCTN 3	Sept 1984	The response of a simple thermodynamic sea-ice model to GCM forcing appropriate for perennial sea-ice. M Bottomley
DCTN 4	Sept 1984	Potential vorticity in the stratosphere derived using data from satellites. S A Clough, N S Grahame and A O'Neill
DCTN 5	Sept 1984	Simulation of the seasonal cycle of SST using globally specified climatological data to force simple ocean models. N S Grahame
DCTN 6	Sept 1984	Development of an improved GCM radiation scheme. A Slingo and R C Wilderspin
DCTN 7	Sept 1984	On the specification of surface fluxes in coupled atmosphere/ocean general circulation models. J F B Mitchell, C A Wilson and C M Price
DCTN 8	Sept 1984	A survey of possible repercussions of the Soviet river reversal programme on Arctic sea-ice. H Cattle
DCTN 9	Oct 1984	A study of a strong stratospheric warming during January 1982 T D A Fairlie
DCTN 10	Nov 1984	An intercomparison of the Met O 11 N45 model and the Met O 20 11-level model on the Cyber 205 J F Dyson
DCTN 11	Nov 1984	Simulation of observed time series of temperature and precipitation over eastern England. D N Reed
DCTN 12	Nov 1984	Forecasts and analyses of the onset of the Southwest monsoon. R Kershaw
DCTN 13	Nov 1984	On modelling the effects of CO_2 on climate. J F B Mitchell
DCTN 14	Dec 1984	Development of a revised longwave radiation scheme for an atmospheric general circulation model. A Slingo and R C Wilderspin
DCTN 15	Jan 1985	Rossby wavetrains in the stratosphere forced by localised disturbances in the troposphere. C J Marks (Oxford), A O'Neill and V D Pope

DYNAMICAL CLIMATOLOGY TECHNICAL NOTES

DCTN 16	Jan 1985	Observing system experiments using the Meteorological Office's 15-level model. R A Bromley
DCTN 17	Feb 1985	Atmospheric general circulation simulation of the climate of the Mediterranean region. H Cattle
DCTN 18	Feb 1985	Diurnal variation and cloud in a general circulation model. C A Wilson and J F B Mitchell
DCTN 19	Feb 1985	The sensitivity of the Saharan region in a general circulation model. W M Cunnington and P R Rowntree
DCTN 20	Mar 1985	The impact of aircraft observations on analyses and forecasts from the operational 15-level model. B R Barwell
DCTN 21	Mar 1985	Non-linear effects on heat-induced circulation of the tropical atmosphere. A E Gill and P J Phlips
DCTN 22	Apr 1985	Simulation of cloudiness with the U.K. Meteorological Office 11-layer AGCM. A Slingo and R C Wilderspin
DCTN 23	Apr 1985	An integrated approach to the representation of cloud processes. R N B Smith
DCTN 24	May 1985	Nuclear Winter: Calculations of the shortwave radiative effects of soot aerosols. A Slingo and P Goldsmith
DCTN 25	Jul 1985	Sea ice and the Antarctic winter circulation: a numerical experiment. J F B Mitchell and T S Hills
DCTN 26	Jul 1985	A Budyko-Sellers model for study of ocean-atmosphere interaction. W J Ingram
DCTN 27	Aug 1985	The effect of a shoaling thermocline on equatorially-trapped Kelvin waves. A E Gill and B A King
DCTN 28	Sept 1985	CO_2 climate sensitivity and model dependence of results. J F B Mitchell, C A Wilson and W M Cunnington
DCTN 29	Sept 1985	Handbook of the Meteorological Office 11-layer atmospheric general circulation model. Volume 1 : Model Description Edited by A Slingo
DCTN 30	Sept 1985	Impact of land surface variations on African rainfall in general circualation models. P R Rowntree, M F Wilson and A B Sangster

DYNAMICAL CLIMATOLOGY TECHNICAL NOTES

DCTN 31	Nov 1985	The annual cycle of sea level in the eastern tropical Pacific. G R Bigg and A E Gill
DCTN 32	Nov 1985	An analytic model of the heat-induced tropical circulation in the presence of a mean wind. P J Phlips and A E Gill
DCTN 33	Nov 1985	The effect of resolution and diffusion on the simulated climate. J F Dyson
DCTN 34	Jan 1986	Rossby adjustment over a step. M K Davey, A E Gill, E R Johnson and P F Linden
DCTN 35	Jan 1986	Issues concerning the evaluation of effective surface roughness of heterogeneous terrain. D J Carson
DCTN 36	Mar 1986	Climate sensitivity and past climates : evidence from numerical studies J F B Mitchell
DCTN 37	Mar 1986	Parametrizations of land-surface processes in Meteorological Office numerical weather prediction and climate models D J Carson
DCTN 38	Apr 1986	Modelling of land-surface processes and their influence on European Climate D A Warrilow, A B Sangster and A Slingo
DCTN 39	Apr 1986	Simulation of climatic change due to increased CO_2 J F B Mitchell
DCTN 40	May 1986	On the interpretation of the Eliassen-Palm flux divergence. **Part I :** Theory D G Andrews
DCTN 41	June 1986	Experiments on tropical circulation with a simple moist model. M K Davey and A E Gill
DCTN 42	Jun 1986	Parameter regimes for studying isolated eddies. P D Killworth and M K Davey